Modulation of sarcoplasmic reticulum Ca^{2+} release in skeletal muscle expressing ryanodine receptor impaired in regulation by calmodulin and S100A1

Naohiro Yamaguchi, Benjamin L. Prosser, Farshid Ghassemi, Le Xu, Daniel A. Pasek, Jerry P. Eu, Erick O. Hernández-Ochoa, Brian R. Cannon, Paul T. Wilder, Richard M. Lovering, David Weber, Werner Melzer, Martin F. Schneider and Gerhard Meissner

Am J Physiol Cell Physiol 300:C998-C1012, 2011. First published 2 February 2011; doi:10.1152/ajpcell.00370.2010

Am J Physiol Cell Physiol 300: C998–C1012, 2011.
First published February 2, 2011; doi:10.1152/ajpcell.00370.2010.

Modulation of sarcoplasmic reticulum Ca^{2+} release in skeletal muscle expressing ryanodine receptor impaired in regulation by calmodulin and S100A1

Naohiro Yamaguchi,[1]* Benjamin L. Prosser,[2]* Farshid Ghassemi,[1]* Le Xu,[1] Daniel A. Pasek,[1] Jerry P. Eu,[3] Erick O. Hernández-Ochoa,[2] Brian R. Cannon,[2] Paul T. Wilder,[2] Richard M. Lovering,[4] David Weber,[2] Werner Melzer,[5] Martin F. Schneider,[2] and Gerhard Meissner[1]

[1]*Department of Biochemistry and Biophysics, School of Medicine, University of North Carolina, Chapel Hill, North Carolina;* [2]*Department of Biochemistry and Molecular Biology, University of Maryland School of Medicine, Baltimore, Maryland;* [3]*Department of Medicine, Division of Pulmonary, Allergy and Critical Care, Duke University, Durham, North Carolina;* [4]*Department of Orthopaedics, University of Maryland School of Medicine, Baltimore, Maryland; and* [5]*Institute of Applied Physiology, Ulm University, Ulm, Germany*

Submitted 8 September 2010; accepted in final form 29 January 2011

Yamaguchi N, Prosser BL, Ghassemi F, Xu L, Pasek DA, Eu JP, Hernández-Ochoa EO, Cannon BR, Wilder PT, Lovering RM, Weber D, Melzer W, Schneider MF, Meissner G. Modulation of sarcoplasmic reticulum Ca^{2+} release in skeletal muscle expressing ryanodine receptor impaired in regulation by calmodulin and S100A1. *Am J Physiol Cell Physiol* 300: C998–C1012, 2011. First published February 2, 2011; doi:10.1152/ajpcell.00370.2010.—In vitro, calmodulin (CaM) and S100A1 activate the skeletal muscle ryanodine receptor ion channel (RyR1) at submicromolar Ca^{2+} concentrations, whereas at micromolar Ca^{2+} concentrations, CaM inhibits RyR1. One amino acid substitution (RyR1-L3625D) has previously been demonstrated to impair CaM binding and regulation of RyR1. Here we show that the RyR1-L3625D substitution also abolishes S100A1 binding. To determine the physiological relevance of these findings, mutant mice were generated with the RyR1-L3625D substitution in exon 74, which encodes the CaM and S100A1 binding domain of RyR1. Homozygous mutant mice (*Ryr1*$^{D/D}$) were viable and appeared normal. However, single RyR1 channel recordings from *Ryr1*$^{D/D}$ mice exhibited impaired activation by CaM and S100A1 and impaired CaCaM inhibition. Isolated flexor digitorum brevis muscle fibers from *Ryr1*$^{D/D}$ mice had depressed Ca^{2+} transients when stimulated by a single action potential. However, during repetitive stimulation, the mutant fibers demonstrated greater relative summation of the Ca^{2+} transients. Consistently, in vivo stimulation of tibialis anterior muscles in *Ryr1*$^{D/D}$ mice demonstrated reduced twitch force in response to a single action potential, but greater summation of force during high-frequency stimulation. During repetitive stimulation, *Ryr1*$^{D/D}$ fibers exhibited slowed inactivation of sarcoplasmic reticulum Ca^{2+} release flux, consistent with increased summation of the Ca^{2+} transient and contractile force. Peak Ca^{2+} release flux was suppressed at all voltages in voltage-clamped *Ryr1*$^{D/D}$ fibers. The results suggest that the RyR1-L3625D mutation removes both an early activating effect of S100A1 and CaM and delayed suppressing effect of CaCaM on RyR1 Ca^{2+} release, providing new insights into CaM and S100A1 regulation of skeletal muscle excitation-contraction coupling.

Ca^{2+} release channel; excitation-contraction coupling; *Ryr1*$^{D/D}$ mouse; RyR1-L3625D

THE SARCOPLASMIC RETICULUM (SR) is an intracellular organelle that plays a key role in striated muscle contraction and relaxation by releasing and resequestering Ca^{2+} from the myoplasm. A Ca^{2+} release channel known as the ryanodine receptor (RyR) and an ATP-driven Ca^{2+} pump are the two principal transport systems responsible for the release and uptake of Ca^{2+} (7, 8, 18). In excitation-contraction (EC) coupling of skeletal muscle, an action potential initiates L-type Ca^{2+} channel (Cav1.1) conformational changes that lead to the activation of the skeletal muscle RyR (RyR1) via a direct interaction, the release of Ca^{2+} from the SR, and muscle contraction (33).

RyR1 is the major ryanodine receptor isoform in skeletal muscle (12). Both transcriptional and posttranscriptional mechanisms contribute to the coordinated assembly of the functional Cav1.1-RyR1 complex (31). RyR1 is a large ion channel composed of four 560-kDa peptide subunits, four 12-kDa FK506 binding proteins, and multiple associated proteins that include calmodulin (CaM) and S100A1. Both the Ca^{2+}-free (apoCaM) and Ca^{2+}-bound (CaCaM) forms of CaM bind with nanomolar affinity to RyR1 (2). CaM activates RyR1 at submicromolar Ca^{2+} concentrations and inhibits RyR1 at micromolar Ca^{2+} concentrations. Mutagenesis, peptide studies, and cryo-electron microscopy indicate that apoCaM and CaCaM bind to an overlapping region (amino acid residues 3614–3643) distal to the ion pore of RyR1 (30, 32, 50). This suggests that CaM exerts its effects allosterically through long-range interactions within RyR1.

Insights into the cellular regulation of RyR1 by CaM have been obtained by expressing two RyR1 mutants in RyR1-deficient (dyspedic) myotubes (22). Neither RyR1-L3624D deficient in apoCaM and CaCaM binding nor RyR1-W3620A deficient in only CaCaM binding eliminated voltage-gated SR Ca^{2+} release. On the other hand, studies with permeabilized adult mouse skeletal myofibers suggested that CaM regulation of RyR1 may have a role in skeletal muscle EC coupling (29). CaM decreased the frequency and size of Ca^{2+} sparks, whereas a Ca^{2+}-insensitive mutant of CaM increased both spark frequency and amplitude. However, the physiological relevance of eliminating the interaction of CaM with RyR1 is unclear.

S100A1 is a member of the S100 Ca^{2+} binding protein family that regulates SR Ca^{2+} release and mitochondrial function in many tissues including cardiac and skeletal muscle (11, 46). S100A1 bound to several RyR1 fragments and activated the receptor at nanomolar Ca^{2+} concentrations (43). Competition studies with CaM and binding experiments with an RyR1

* N. Yamaguchi, B. L. Prosser, and F. Ghassemi contributed equally to this work.

Address for reprint requests and other correspondence: G. Meissner, Dept. of Biochemistry and Biophysics, Univ. of North Carolina, Chapel Hill, NC 27599-7260 (e-mail: meissner@med.unc.edu).

fragment (amino acid residues 3616–3627) (27, 47) revealed that S100A1 binds to the NH_2-terminal region of the CaM binding domain involved in binding the Ca^{2+}-bound form of CaM to RyR1 (17, 30, 50). Intact flexor digitorum brevis (FDB) muscle fibers isolated from S100A1-knockout mice exhibited a decreased Ca^{2+} transient amplitude during a single action potential and decreased SR Ca^{2+} release flux in response to voltage-clamp depolarizations (26, 27). These results suggested that S100A1 potentiates skeletal muscle EC coupling by interacting with the NH_2-terminal region of the RyR1 CaM binding domain.

To better understand the in vivo role of CaM and S100A1 regulation of RyR1, we prepared a genetic strain of mice by homologous recombination expressing a mutant form of RyR1 (RyR1-L3625D or $RyR1^D$). We showed previously that the homologous mutation L3624D in rabbit RyR1 reduces CaM binding affinity and CaM regulation of recombinant RyR1 expressed in human embryonic kidney (HEK) 293 cells (50). Leu-3625 is located on the hydrophobic side of an amphipathic helix involved in RyR1 binding of both CaCaM and CaS100A1 (17, 47). In the present study, the physiological effects of impaired regulation of RyR1 by CaM and S100A1 were examined using isolated skeletal muscle membrane and fiber preparations from *Ryr1*$^{D/D}$ mice, and by evaluating whole muscle contractility in vivo. The present and previous results indicate that the predominant modulatory effects of S100A1 or CaM binding to this domain of RyR1 in skeletal muscle are *1*) a potentiation of SR Ca^{2+} release by S100A1 during a single action potential or initial depolarization; and *2*) a suppression of release by delayed inhibition of SR Ca^{2+} release by CaCaM during repetitive action potentials or prolonged depolarization. These opposing early activating effects of S100A1 and later inhibitory effects of CaCaM on SR Ca^{2+} release are both eliminated in the *Ryr1*$^{D/D}$ mice. These studies provide insight into how CaM and S100A1 binding to RyR1 tunes SR Ca^{2+} release to differentially regulate EC coupling.

EXPERIMENTAL PROCEDURES

Materials. [^{3}H]ryanodine was obtained from Perkin Elmer Life Sciences, protease and phosphatase inhibitor cocktails from Sigma, and phospholipids from Avanti Polar Lipids. Other chemicals were from Sigma-Aldrich unless specified otherwise.

Preparation of mutant mice. Mouse *Ryr1* gene was kindly provided by Dr. Jonathan Stamler (Case Western Reserve University, Cleveland, OH). Multiple base changes in exon 74 that encodes the CaM and S100A1 binding domain were introduced by pfu polymerase-based chain reaction using mutagenic oligoprimers and the QuikChange site-directed mutagenesis kit (Stratagene). A 7.7-kb fragment with the mutation (L3625D, D mutation) and 1.2-kb fragment were cloned into pBR322 containing the neomycin-resistant gene flanked by loxP sites and thymidine kinase gene (Fig. 1). Mutant mice carrying the RyR1-L3625D mutation (RyR^D) were prepared using established methods (4). Briefly, linearized targeting vector was transfected into embryonic stem (ES) cells (cell line E14) by electroporation. Cells containing the recombinant gene were selected in presence of G418 and gancyclovir. ES cell clones were screened by PCR and Southern blotting, and mutations were confirmed by sequencing. Targeted ES cells were injected into blastocysts of C57BL/6J mice in the Animal Models Core Facility of University of North Carolina at Chapel Hill. A male chimera mouse carrying the RyR1-L3625D mutation was mated with a 129/SvEv female mouse to obtain heterozygous offspring. Targeting construct also carried the Cre recombinase gene driven by a testis-specific angiotensin-converting enzyme promoter. Therefore, germ line transmission of the mutation to heterozygous offspring caused removal of the gene cassette flanked by loxP sites (5). Homozygous gene-targeted animals (*Ryr1*$^{D/D}$) were obtained by mating heterozygous mice (*Ryr1*$^{+/D}$). Experiments were performed with mice at least 5 times back-crossed to 129/SvEv genetic background. Offspring were genotyped by PCR followed by restriction digestion with *Hin*fI. The mice were handled according to the National Institutes of Health guidelines for the use and care of experimental animals. All experiments were approved by the Institutional Animal Care and Use Committees of University of North Carolina at Chapel Hill and University of Maryland.

Preparation of membrane fractions. Leg skeletal muscle was homogenized in 0.02 M imidazole, pH 7.0, 0.3 M sucrose, 0.15 M NaCl, 0.1 mM EGTA, protease inhibitors (Sigma), and 1 mM glutathione (oxidized form), using a Tekmar Tissumizer for 2 × 7 s at a setting of 13,500 rpm. Homogenates were centrifuged for 45 min at 35,000 rpm in a Beckman Ti75 rotor, and pellets were resuspended in the above buffer without EGTA and glutathione to obtain a crude membrane fraction. Membranes were stored in small aliquots at −80°C.

Single-channel recordings. Single-channel measurements of wild-type (WT) and mutant RyR1s were performed in planar lipid bilayers as described with some modifications (51). Crude skeletal muscle membrane fractions containing WT and mutant RyR1s were pretreated for 30 min with 1 μM myosin light chain kinase-derived CaM binding peptide to facilitate dissociation of endogenous CaM (1). The final peptide concentration was 10 nM after the addition of membranes to the *cis*, cytosolic chamber of the bilayer apparatus. A strong dependence of single-channel activities on *cis* Ca^{2+} concentration indicated that the large cytosolic "foot" region faced the *cis* chamber of the bilayers. The trans SR luminal side of the bilayer was defined as ground. Measurements were made with symmetrical 0.25 M CsCl, 20 mM CsHepes, pH 7.4, with the indicated concentrations of Ca^{2+} and ATP. Exogenous CaM and S100A1 were added to the *cis*, cytosolic solution. Electrical signals were filtered at 2 kHz, digitized at 10 kHz, and analyzed as described (48). Channel open probabilities (P_o) were obtained from 2-min recordings by setting the threshold level at 25% and 50% of the current amplitude between the closed (c) and open (o) channel states. P_o values in multichannel recordings were calculated using the equation $P_o = \sum i P_{o,i}/N$, where N is the total number of channels and $P_{o,i}$ is channel open probability of the ith channel.

[^{3}H]ryanodine binding. [^{3}H]ryanodine binding experiments were performed with crude membrane fractions isolated from skeletal muscle. Unless otherwise indicated, membranes were incubated at 24°C with 2.5 nM [^{3}H]ryanodine in 20 mM imidazole, pH 7.0, 0.15 M sucrose, 250 mM KCl, 5 mM glutathione (reduced), protease inhibitors, and the indicated Ca^{2+} and CaM concentrations. Endogenous CaM was removed by the addition of 0.1–0.2 μM myosin light chain kinase-derived CaM binding peptide (1). Nonspecific binding was determined using a 1,000- to 2,000-fold excess of unlabeled ryanodine. After 20 h, samples were diluted with 8 volumes of ice-cold water and placed on Whatman GF/B filters preincubated with 2% polyethyleneimine in water. Filters were washed with three 5-ml volumes of ice-cold 0.1 M KCl, and 1 mM KPipes, pH 7.0. Radioactivity remaining with the filters was determined by liquid scintillation counting to obtain bound [^{3}H]ryanodine.

Maximal specific binding capacity (B_{max}) values of [^{3}H]ryanodine binding were determined by incubation of membranes for 4 h at 24°C with a near to saturating concentration of [^{3}H]ryanodine (20 nM) in 20 mM imidazole, pH 7.0, 0.6 M KCl, 0.15 M sucrose, 1 mM glutathione (oxidized), protease inhibitors, and 0.1 mM Ca^{2+}. Specific binding was determined as described above.

$^{45}Ca^{2+}$ uptake. ATP-dependent $^{45}Ca^{2+}$ uptake by crude membrane fractions was determined by filtration (49). $^{45}Ca^{2+}$ uptake was initiated by placing membranes in 0.15 M KCl-20 mM imidazole, pH 7.0, containing 5 mM ATP, 8 mM Mg^{2+}, 5 mM Koxalate (a Ca^{2+} precipitating agent to increase Ca^{2+} uptake capacity), 10 μM ruthe-

nium red (to inhibit RyR1), 5 mM NaN_3 (to inhibit mitochondrial Ca^{2+} uptake), 1 mM EGTA, Ca^{2+}, and $^{45}Ca^{2+}$ to yield a 0.5–0.6 μM free Ca^{2+} concentration. To obtain $^{45}Ca^{2+}$ uptake rates, aliquots were placed at 2, 4, and 6 min on 0.45-μM Millipore filters under vacuum and rinsed with three 3-ml volumes of ice-cold 0.175 M KCl, 5 mM imidazole, pH 7.0. Radioactivity remaining with the vesicles on the filters was determined by liquid scintillation counting.

Isothermal titration calorimetry. Peptide binding to CaS100A1 was examined via isothermal titration calorimetry (ITC), using a VP-ITC titration microcalorimeter (MicroCal, Northhampton, MA; General Electric) as described (27, 47). For ITC, all S100A1 and peptide solutions were degassed under vacuum for 5 min and equilibrated at 37°C before use. The reference cell contained double-distilled H_2O, and the sample cell (1.4 ml) contained 50 mM HEPES, pH 7.2, 15 mM NaCl, 10 mM $CaCl_2$, and 50 μM S100A1. Upon equilibration, a 2 mM (WT) or 5 mM (mutant) peptide solution prepared in the same buffer as above (without S100A1) was injected in 5-μl aliquots with a 300-s interval between each injection. Data were fit using ITC software provided by the vendor. S100A1 was prepared as described (27, 47). Synthetic peptides were purchased from Biosynthesis (Lewisville, TX) with their amino termini acetylated (ac−) and their COOH termini amidated (−am). Concentrations and composition were confirmed using amino acid analyses. These include the wild-type RyRP12 peptide derived from residues 3617–3628 of RyR1 (ac-KKAVWHKLLSKQ-am) and mutant RyRP12 peptides (ac-KKAVWHKLDSKQ-am; ac-KKAVDHKLLSKQ-am; ac-KKAVD-HKLDSKQ-am); mutations are underlined.

FDB fiber preparation. Fibers were prepared using enzymatic dissociation of FDB muscles of 1.5-mo-old *Ryr1*$^{+/+}$ and *Ryr1*$^{D/D}$ mice and were cultured as described (13). After ~24 h in minimal essential medium, fiber culture medium was changed to 2 ml Ringer solution (135 mM NaCl, 4 mM KCl, 1 mM $MgCl_2$, 10 mM HEPES pH 7.4, 10 mM glucose, 1.8 mM $CaCl_2$).

Monitoring single-fiber Ca^{2+} transients using Indo-1 ratiometric recordings or high-speed confocal microscopy with Fluo-4. FDB fiber loading with Indo-1 AM, ratiometric recording, image sampling, and data analysis were performed as described (27). Similarly, Fluo-4-AM loading, high-speed linescan *x-t* imaging on a Zeiss LSM 5 Live confocal system, and image analysis were performed as described (27). Multiple stimulation paradigms were performed as described in RESULTS.

Calculation of SR Ca^{2+} release flux from Fluo-4-AM fluorescence recordings. Fluo-4 fluorescence recordings (F) and baseline fluorescence (F_0) were converted to ratio signals [$R = (F - F_0)/F_0$]. To derive the free Ca^{2+} concentration according to *Eq. 1*, we assumed $K_{D,fluo} = 1$ μM which is within the range of estimates for myoplasmic conditions (9) and $k_{off,fluo} = 90\ s^{-1}$ (37).

$$\left[Ca^{2+}\right] = K_{D,fluo}\left[\left(1/k_{off,fluo}\right)\left(dR/dt\right) + R - R_{min}\right]/\left(R_{max} - R\right) \quad (1)$$

The fluorescence ratio at saturating Ca^{2+} concentration R_{max} was determined for each individual fiber using ionomycin permeabilization (5 μM). The ratio at zero Ca^{2+} concentration ([Ca^{2+}]) R_{min} was calculated using *Eq. 2*. Because the extracellular Ca^{2+} concentration ([Ca^{2+}]$_o$) of resting free Ca^{2+}, determined in separate experiments using the indicator dye Indo-1, was not significantly different in WT and mutant fibers, we used the average of 77 nM for all calculations.

$$R_{min} = -R_{max}\left[Ca^{2+}\right]_o/K_D \quad (2)$$

To determine Ca^{2+} release underlying action potential-induced Fluo-4 fluorescence transients, we used a pulse paradigm consisting of a single stimulus followed (after 400 ms) by five sequential tetani at 100 Hz (200 ms each) applied at intervals of 200 ms. This protocol provides six long relaxation intervals after the single pulse and following the tetani that can be used to characterize Ca^{2+} removal (19, 20, 42). After data reduction by averaging every five consecutive sample points, traces were smoothed using an adaptive digital filter (35). A Ca^{2+} removal model including binding and transport was used to simultaneously fit the relaxation phases in the long intervals and in the 700-ms recording period following the last tetanus. Binding to Ca^{2+}-specific sites of troponin C (T-sites) and parvalbumin-like Ca^{2+}-Mg^{2+} sites (P-sites) was calculated as described (3). Binding site concentrations and rate constants of troponin and parvalbumin were adopted from Baylor and Hollingworth (3). The rate constants were adjusted to our experimental temperature of 20°C by linear interpolation of the values at 16°C and 28°C published in that study. Fast Ca^{2+} binding to ATP was described by a component proportional to free Ca^{2+} [scaling factor $F = 3.6$; (3)]. Ca^{2+} removal by transport (e.g., uptake by the SR Ca^{2+}-ATPase) was assumed to be proportional to free [Ca^{2+}] (rate constant k_{uptake}). The rate constant values used for the calculations were for T-sites: $k_{on,T,Ca} = 115$ μM/s, $k_{off,T,Ca} = 150\ s^{-1}$; and for P-sites: $k_{on,P,Ca} = 54.0$ μM/s, $k_{off,P,Ca} = 0.65\ s^{-1}$, $k_{on,P,Mg} = 0.043$ μM/s, $k_{off,P,Mg} = 3.9\ s^{-1}$, $k_{uptake} = 1{,}000\ s^{-1}$. $[T]_{tot}$ and $[P]_{tot}$, the total concentrations of T-sites and P-sites, were 0.240 mM and 1.5 mM, respectively. After an initial calculation with these parameters, $k_{on,P,Mg}$ and k_{uptake} were adjusted by iteration to minimize the least squares deviation between calculated and measured fluorescence ratio in the six relaxation phases.

The fit started ~20 ms after the end of the depolarization to account for the time required to turn off Ca^{2+} release. The Ca^{2+} occupancies of all model compartments [T-sites, P-sites, ATP (F-sites) and uptake] were summed, and the release flux was calculated as the time derivative of the sum. Calculations were performed using Euler's method (36). Analysis software was written in Delphi (Borland) and Visual Basic for Excel (Microsoft).

Ca^{2+} transient recording and calculation of Ca^{2+} release flux during pulse depolarization of single voltage-clamped muscle fibers. All solutions used for single muscle fiber voltage-clamp experiments were identical to those used previously (25), except for the addition of 50 μM Fluo-4 to the internal solution in the patch pipette to monitor Ca^{2+} transients. Fluorescence signals were recorded during voltage-clamp depolarizations using a high-speed confocal system (Zeiss LSM 5 LIVE) synchronized with the patch-clamp system (26). Ca^{2+} release flux from voltage clamp-elicited Fluo-4 transients was calculated as described (26).

Contractile function. As a measure of whole muscle force production, we recorded tension generated by the tibialis anterior (TA) muscle in vivo, as previously described (14). Briefly, the distal TA tendon of anesthetized animals was surgically released and attached to a load cell. A 26-gauge needle was then inserted through the proximal tibia to stabilize the leg. The load cell was adjusted via a micromanipulator to stretch the muscle to a set resting length (11 mm). TA contraction was then triggered via subcutaneous stimulation of the peroneal nerve, and the resulting force generated was sampled at 1 kHz and analyzed with Polyview acquisition software. We utilized several stimulation protocols, which are detailed in RESULTS, to evaluate force generation. Following contractile function experiments, animals were euthanized and the TAs were isolated and weighed. As muscle length was fixed in all experiments, and muscle density was assumed to be a constant 1.06 mg/mm^3, physiological cross-sectional area (PCSA = mass/density × length) of the TA was solely a function of muscle mass. Force (F) was therefore normalized to TA mass to calculate specific force, P_0 = F/PCSA.

Biochemical assays and data analyses. Free Ca^{2+} concentrations were obtained by including the appropriate amounts of Ca^{2+} and EGTA determined using stability constants and a published computer program (34). Free Ca^{2+} concentrations were verified with the use of a Ca^{2+}-selective electrode. Results are given as mean ± SE. Differences between two genotypes were analyzed with Student's *t*-test.

RESULTS

CaM is a small cytoplasmic Ca^{2+} binding protein that binds with nanomolar affinity to the skeletal muscle ryanodine receptor (RyR1) in the absence and presence of Ca^{2+}. Each subunit of the intact tetrameric receptor has a single CaM binding domain for the Ca^{2+}-free (apoCaM) and Ca^{2+}-bound (CaCaM) forms of CaM (2). We showed previously that in the presence of 0.1–0.2 and 100 μM Ca^{2+}, the single L3624D substitution in rabbit RyR1 reduced CaM binding affinity and regulation of recombinant RyR1 expressed in HEK 293 cells (50). In the present study, we generated by homologous recombination a mouse with the corresponding substitution (L3625D) in RyR1 ($RyR1^D$) (Fig. 1). The mutation did not noticeably alter the appearance, general behavior, body weight, or lifespan of the $Ryr1^{D/D}$ mice, which suggested that the possibility of long-term or nonspecific effects of the mutation in muscle or other tissues was minimal. $Ryr1^{+/+}$ (WT), $Ryr1^{+/D}$, and $Ryr1^{D/D}$ mice all lived longer than 9 mo.

CaM regulation of RyR1 isolated from $Ryr1^{+/+}$ and $Ryr1^{D/D}$ mice. The efficiency of the $RyR1^D$ mutation in eliminating the regulation of RyR1 by CaM was probed in single-channel measurements (Fig. 2). Membranes isolated from the leg muscle of $Ryr1^{+/+}$ and $Ryr1^{D/D}$ mice were fused with a lipid bilayer. Fig. 2, *A* and *B*, shows representative single-channel recordings of $Ryr1^{+/+}$ (*left*) and $Ryr1^{D/D}$ (*right*). Channels were recorded in 0.25 M CsCl on both sides of the bilayer with 0.2 μM (Fig. 2*A*) or 7 μM (Fig. 2*B*) free Ca^{2+} in the *cis*, cytosolic bilayer chamber. To increase open channel probability (P_o), channels were recorded in the presence of 1 mM ATP (18). Single-channel recordings typically showed variable subconductances, in addition to full openings with conductance of 509 ± 12 pS (n = 19) for $Ryr1^{+/+}$ and 495 ± 14 pS (n = 17) for $Ryr1^{D/D}$. To account for the majority of channel openings, channel open probabilities were calculated by setting the threshold level at 25% and 50% of the current amplitude between the closed (c) and open (o) channel states (Fig. 2). In the absence of CaM, there were no significant differences in P_o between $Ryr1^{+/+}$ and $Ryr1^{D/D}$ channels at 0.2 and 7 μM *cis* free Ca^{2+} (Fig. 2 legend). Addition of 20 and 200 nM CaM to the *cis* side of the bilayer increased activity of $Ryr1^{+/+}$ channels at 0.2 μM free Ca^{2+}, as indicated by an increase in P_o (Fig. 2*A*). The average P_o of nine single and multiple $Ryr1^{+/+}$ channel recordings at 0.2 μM Ca^{2+} increased by ~150% of the control with 20 nM and to ~165% with 200 nM CaM in the *cis* chamber (Fig. 2*A*, *bottom left*). Addition of 20 nM CaM did not activate $Ryr1^{D/D}$, whereas 200 nM CaM significantly activated the mutant channels (Fig. 2*A*, *bottom right*). At 7 μM free Ca^{2+}, WT but not mutant channels were significantly inhibited by 20 nM CaM (Fig. 2*B*). Both types of channels were inhibited by the addition of 200 nM CaM to the *cis* side of the bilayer.

The effects of the $RyR1^D$ mutation on the interaction of CaM and RyR1 were also examined in a ligand binding assay, using the RyR-specific probe ryanodine (Fig. 3). [^{3}H]ryanodine

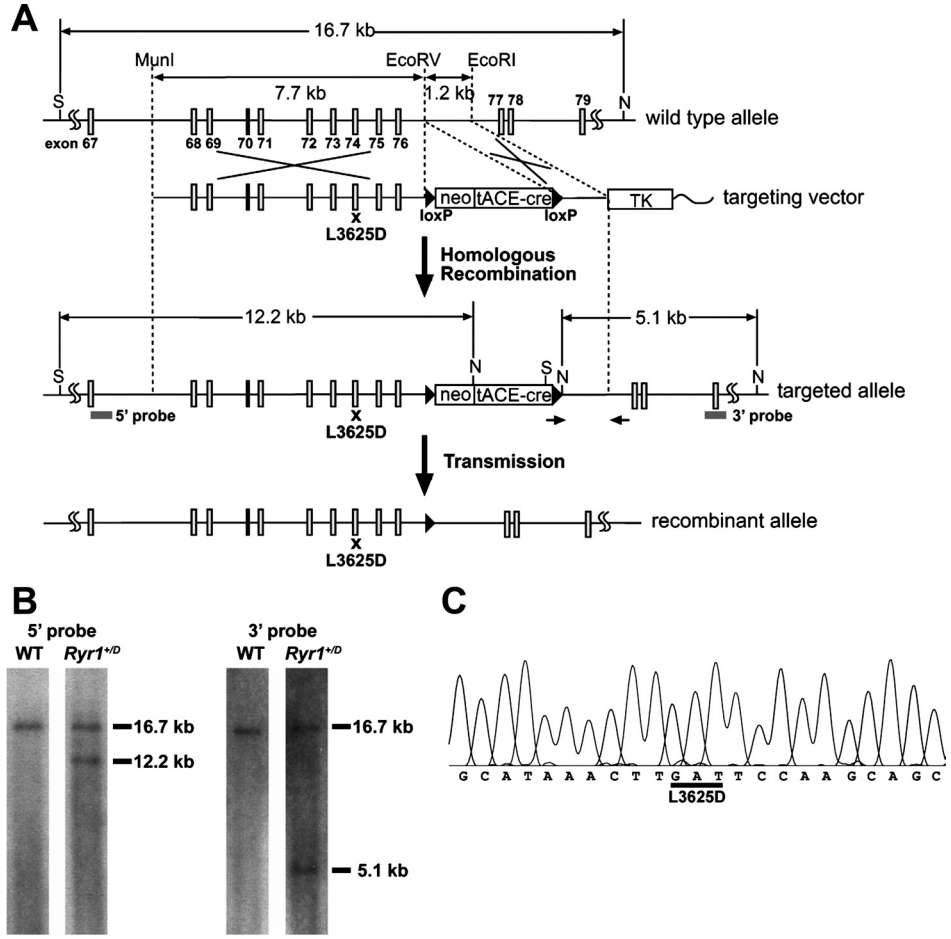

Fig. 1. Generation of mice with an L3625D mutation in the calmodulin (CaM)-binding site of ryanodine receptor 1 (RyR1). *A*: schematic representation of the mouse *Ryr1* gene and targeting construct. S and N represent *Spe*I and *Nde*I restriction enzyme sites, respectively. neo, tACE-cre, and TK denote neomycin-resistant gene, Cre recombinase gene driven by testis-specific angiotensin-converting enzyme promoter, and thymidine kinase gene, respectively. Arrows and "x" indicate the position of primers for screening and a mutation site, respectively. *B*: southern blot analysis of genomic DNA. After restriction enzyme digestion of genomic DNA with *Spe*I and *Nde*I, 5′- and 3′-probes identify 12.2-kb and 5.1-kb fragment in targeted allele, respectively. Both probes hybridize with 16.7-kb fragments in wild-type (WT) allele. *C*: sequence analysis of RT-PCR. cDNA encoding CaM-binding site of RyR1 was amplified from total RNA from homozygous (hybrid genetic background) mouse skeletal muscle and sequenced. The L3625D mutation was confirmed. A *Hin*fI site created by the L3625D mutation (GATTC) was used for screening the mutant allele.

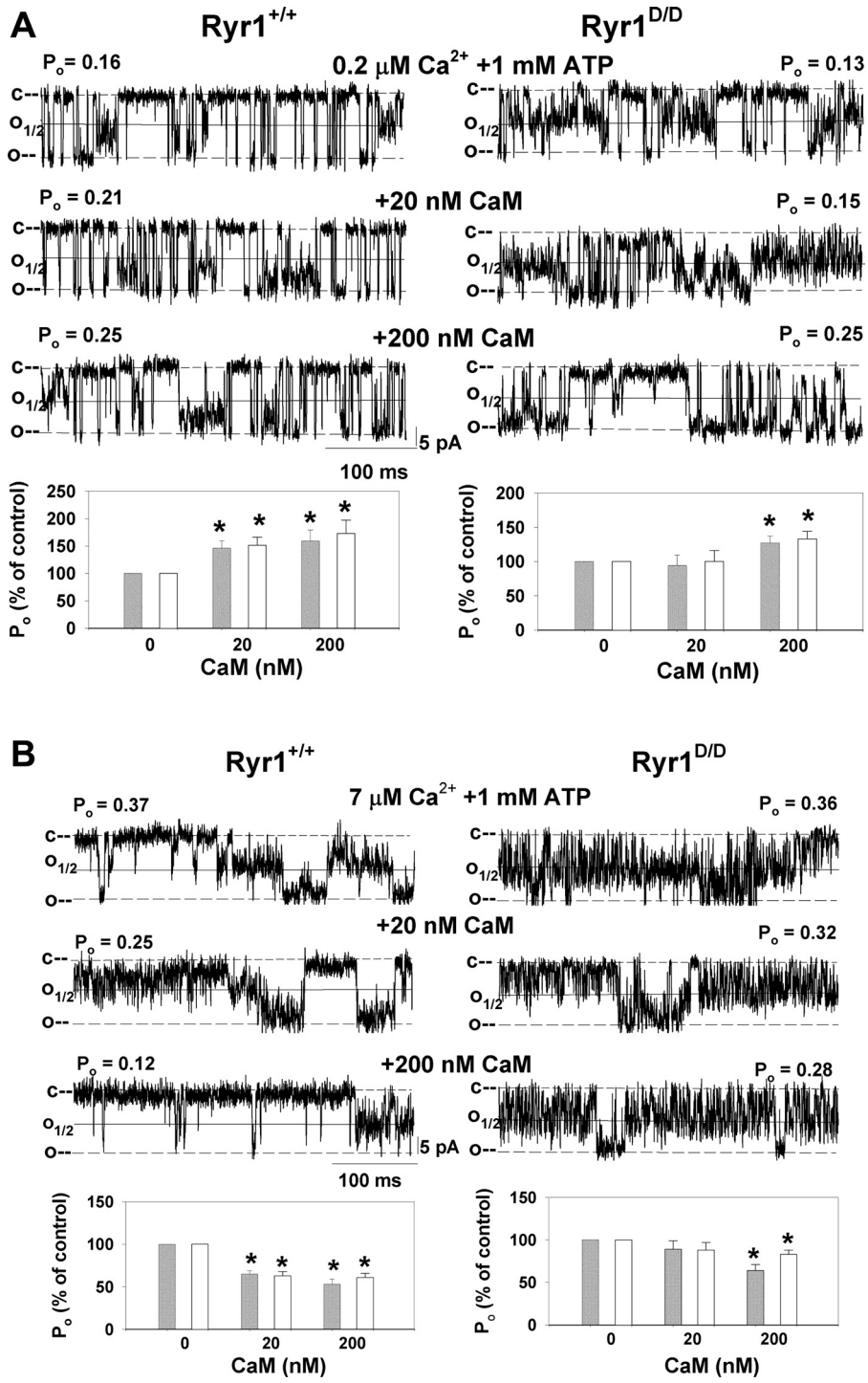

Fig. 2. Effects of CaM on single $Ryr1^{+/+}$ and $Ryr1^{D/D}$ channel activities. Membranes isolated from skeletal muscle of $Ryr1^{+/+}$ and $Ryr1^{D/D}$ mice were fused with lipid bilayer as described in EXPERIMENTAL PROCEDURES. Representative single-channel currents (downward deflections from closed levels, c–) were recorded at −35 mV at 0.2 μM (*A*) and 7 μM (*B*) *cis*, cytosolic free Ca^{2+} in the presence of 1 mM ATP as described in EXPERIMENTAL PROCEDURES in the absence of CaM (*top* traces) and following the addition of 20 nM (*middle* traces) and 200 nM (*bottom* traces) *cis* CaM. Channel open probabilities (P_o) obtained from 2-min recordings in the absence of CaM were 0.15 ± 0.02 (n = 21) and 0.14 ± 0.02 (n = 29) at 50% threshold setting, 0.30 ± 0.04 and 0.23 ± 0.02 at 25% threshold setting at 0.2 μM Ca^{2+} and 1 mM ATP, and 0.27 ± 0.05 (n = 14) and 0.26 ± 0.05 (n = 11) at 50% threshold setting and 0.38 ± 0.05 and 0.48 ± 0.05 at 25% threshold setting at 7 μM Ca^{2+} and 1 mM ATP for $Ryr1^{+/+}$ and $Ryr1^{D/D}$, respectively. Normalized P_o values (*bottom*) were obtained from 2-min recordings by setting the threshold level at 25% (open bars) and 50% (gray bars) of the current amplitude between the closed (c) and open (o) channel states. Data are means ± SE of 9 and 15 (*A*) and 14 and 11 (*B*) channel recordings for $Ryr1^{+/+}$ and $Ryr1^{D/D}$, respectively. *$P < 0.05$ compared with respective control (−CaM).

binds with high specificity to RyR1 and is widely used as a probe for channel activity because of its preferential binding to the open channel state (39). In agreement with single-channel measurements, CaM increased [^{3}H]ryanodine binding to $Ryr1^{+/+}$ membranes at 0.15 μM Ca^{2+} (Fig. 3*A*) and decreased binding at 25 μM Ca^{2+} (Fig. 3*B*). CaM (20–40 nM) did not alter [^{3}H]ryanodine binding to membranes prepared from $Ryr1^{D/D}$ muscle. Elevated concentrations of CaM (190 nM) decreased [^{3}H]ryanodine binding to $Ryr1^{D/D}$ at 25 μM Ca^{2+}. Taken together, single-channel and [^{3}H]ryanodine binding measurements indicate that the RyR1^D mutation decreases the efficiency of CaM regulation of RyR1 at submicromolar and micromolar Ca^{2+} concentrations.

RyR1 residues W3621 and L3625 are important for CaCaM-RyR and CaS100A1-RyR complex formation. In previous studies, RyR1 mutations at W3621 and L3625 significantly decreased the CaCaM-RyR1 interaction (50), which was consistent with the X-ray structure of a complex between a binding domain peptide of RyR1 and CaCaM (Fig. 4, *B* and *D*). Likewise, based on the nuclear magnetic resonance (NMR)-

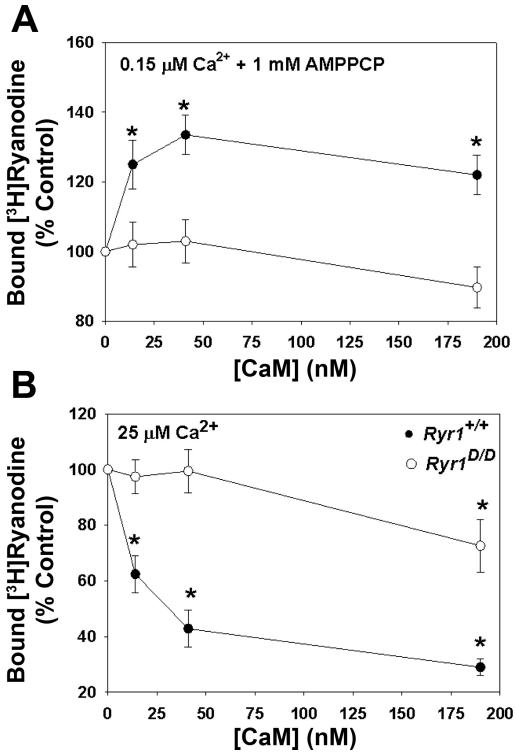

Fig. 3. CaM regulation of RyR1 from skeletal muscle of $Ryr1^{+/+}$ and $Ryr1^{D/D}$ mice. Specific [^{3}H]ryanodine binding to crude membrane fractions from skeletal muscle of $Ryr1^{+/+}$ (●) and $Ryr1^{D/D}$ (○) mice was determined at the indicated CaM concentrations in the presence of 0.15 μM Ca^{2+} and 1 mM AMPPCP (a nonhydrolyzable ATP analog) (*A*) and 25 μM (*B*) free Ca^{2+} as described in EXPERIMENTAL PROCEDURES. Data are means ± SE of 4 experiments. *$P < 0.05$ compared with control (−CaM).

structure of S100A1-RyRP12 (Fig. 4, *A* and *C*), it was not surprising that a 12-residue RyRP12 peptide from this same S100A1/CaM binding domain of the intact RyR1 competed with the full-length RyR1 for binding to CaCaM and CaS100A1 (27, 47, 50). As with the CaCaM-RyR1 peptide X-ray structure (17), the NMR structure of S100A1-RyRP12 illustrates the importance of the hydrophobic face of the amphipathic RyRP12 peptide for complex formation that include residues W3621 and L3625.

To examine this interaction in more detail, binding of CaS100A1 to WT and mutant RyRP12 peptides derived from RyR1 was measured using ITC. In Fig. 4*E*, representative ITC traces are shown together with theoretical fitted curves for the binding of WT and three mutant RyRP12 peptides to CaS100A1. For the WT RyRP12 peptide, binding to CaS100A1 was readily detected ($n = 0.75 \pm 0.12$; $K_D = 75 \pm 12$ μM; $\Delta H = -5.8 \pm 0.6$ kcal/mol). However, data for the L3625D mutant peptide were barely detectable; specifically, the binding was so weak that the stoichiometry could not be quantitatively determined, so it could only be assumed ($n = 1$). Therefore, the ITC data for the L3625D mutant provided only a limiting value for binding ($K_D > 0.9 \pm 0.1$ mM). No detectable binding was observed for the W3621D or the W3621D + L3625D double mutant. Together, the data show that the same RyR1 region, which includes W3621 and L3625, is important for binding both CaCaM and CaS100A1.

S100A1 regulation of RyR1 isolated from $Ryr1^{+/+}$ and $Ryr1^{D/D}$ mice. Next we probed the effect of the RyR1^D mutation in eliminating the regulation of RyR1 by S100A1. Figure 5 shows representative single-channel recordings of $Ryr1^{+/+}$ (*left*) and $Ryr1^{D/D}$ (*right*). Channels were recorded and analyzed as in Fig. 2*A* in the presence of 0.2 μM *cis* Ca^{2+} and 1

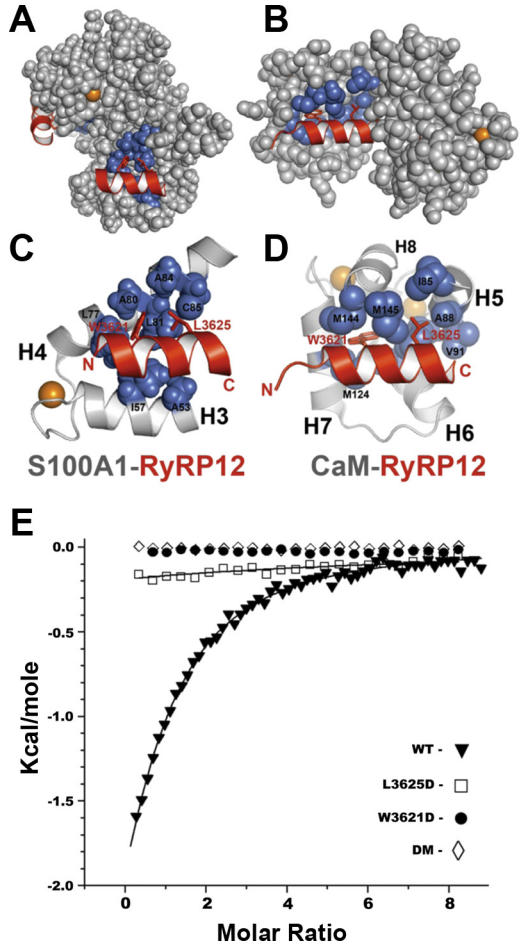

Fig. 4. CaCaM and CaS100A1 bound to the CaM/S100A1-binding domain of RyR1. *A*: space-filling model of dimeric CaS100A1 with each subunit bound to a peptide (RyRP12; shown in red) from the CaM/S100A1-binding domain of RyR1. In the foreground, one subunit is shown illustrating the location of RyR1 residues W3621 and L3625 on the hydrophobic side of an amphipathic helix, which in turn interact with hydrophobic residues on CaS100A1 (shown in blue). *B*: space-filling diagram of CaCaM bound to a peptide (red) from the CaM/S100A1-binding domain of RyR1 illustrating that these two residues (W3621, L3625) also interact directly with hydrophobic residues on CaCaM (shown in blue). *C*: ribbon diagram illustrating a close-up view of the CaS100A1-RyRP12 interaction. *D*: ribbon diagram illustrating a close-up view of the CaCaM-RyR1 peptide interaction. In *A*–*D*, calcium ions are colored orange. *E*: binding of CaS100A1 to WT and mutant RyRP12 peptides derived from RyR1 as determined using isothermal titration calorimetry (ITC). Shown is a representative trace together with a theoretical fitted curve for the binding of the WT-RyRP12 peptide to CaS100A1 (▲). These data were duplicated to provide the thermodynamic binding parameters ($n = 0.75 \pm 0.12$; $K_D = 75 \pm 12$ μM; $\Delta H = -5.8 \pm 0.6$ kcal/mol). Also shown are representative data for the binding of the RyR1-L3625D mutant peptide together with a theoretical curve for binding. In this case, the binding stoichiometry could not be quantitatively determined since the binding was weak and was assumed to be one ($n = 1$) in all the titrations measured; therefore, these data provided only a limiting value for binding (□ $K_D > 0.9 \pm 0.1$ mM). No detectable binding was observed for the RyR1-W3621D (●) or the RyR1-W3621D + L3625D [double mutant (DM); ◇] mutant peptides.

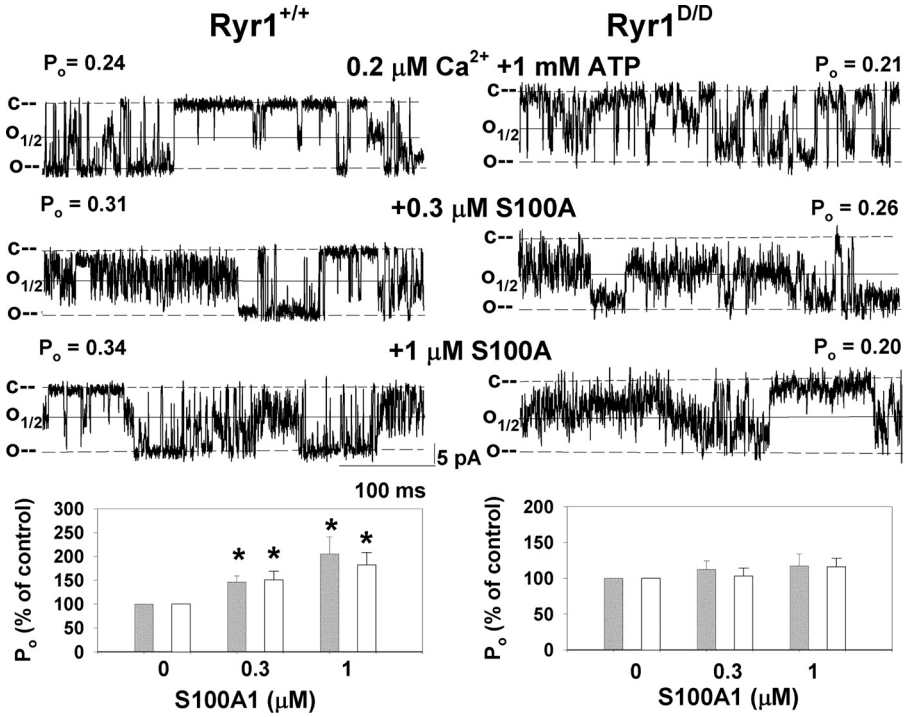

Fig. 5. Effects of S100A1 on single $Ryr1^{+/+}$ and $Ryr1^{D/D}$ channel activities at 0.2 μM Ca^{2+}. Membranes isolated from skeletal muscle of $Ryr1^{+/+}$ (*left*) and $Ryr1^{D/D}$ (*right*) mice were fused with lipid bilayer. Representative single-channel currents (downward deflections from closed levels, c–) were recorded at −35 mV at 0.2 μM *cis*, cytosolic free Ca^{2+} in the presence of 1 mM ATP as described in EXPERIMENTAL PROCEDURES in the absence of S100A1 (*top* traces) and following the addition of 0.3 μM (*middle* traces) and 1 μM (*bottom* traces) S100A1 to the *cis* chamber. Normalized P_o (*bottom*) was obtained from 2-min recordings by setting the threshold level at 25% (open bars) and 50% (gray bars) of the current amplitude between the closed (c) and open (o) channel states. Data are means ± SE of 3–14 channel recordings. *$P < 0.05$ compared with control (−S100A1).

mM ATP in the *cis* cytosolic bilayer chamber. Addition of 0.3 and 1 μM S100A1 to the *cis* side of the bilayer increased P_o of $Ryr1^{+/+}$. The averaged P_o of single and multiple $Ryr1^{+/+}$ channel recordings at 0.2 μM Ca^{2+} was increased by 145% of the control with 0.3 μM S100A1 and by 205% with 1 μM S100A1 in the *cis* chamber (Fig. 5, *bottom left*). Addition of 3 μM S100A1 did not further increase the activity of WT channels (not shown). $Ryr1^{D/D}$ channels were not activated by 0.3 and 1 μM S100A1 (Fig. 5, *bottom right*). At 50 μM cytosolic free Ca^{2+}, addition of 1 μM S100A1 did not significantly alter P_o of $Ryr1^{+/+}$ and $Ryr1^{D/D}$ (not shown).

Skeletal muscle SR Ca^{2+} handling by WT and mutant mice. To determine the SR Ca^{2+} handling properties in mutant mice, $^{45}Ca^{2+}$ uptake rates (a measure of SR Ca^{2+} pump activity) and B_{max} values of [^{3}H]ryanodine binding (a measure of RyR1 protein expression) were measured. The $^{45}Ca^{2+}$ uptake rates by skeletal muscle isolates of 1.5- to 5.5-mo-old $Ryr1^{D/D}$ mice were not significantly altered (Fig. 6*B*). One and a half-month-old $Ryr1^{+/+}$ and $Ryr1^{D/D}$ mice exhibited similar B_{max} values of [^{3}H]ryanodine binding, whereas reduced levels of [^{3}H]ryanodine binding were observed for 3-mo-old (not significant) and 5.5-mo-old (significant) mice (Fig. 6*A*). No significant differences in [^{3}H]ryanodine binding affinity were observed (K_D = 12.8 ± 1.3 nM and 17.7 ± 3.2 nM for mutant and WT muscle isolates, respectively, $n = 5$).

RyR1 is the major ryanodine receptor isoform in skeletal muscle (12). To determine whether the RyR^D mutation increased the mRNA levels of the other two mammalian RyR isoforms RyR2 and RyR3, we used quantitative RT-PCR. The mRNA levels of all three RyR isoforms were increased to a similar extent (1.5- to 2-fold, not significant) in skeletal muscle of $Ryr1^{D/D}$ mice compared with $Ryr1^{+/+}$ mice ($n = 4$). The data suggest that RyR1 remains the predominant ryanodine receptor isoform in the skeletal muscle of the mutant mice.

Action potential evoked Indo-1 Ca^{2+} transients in $Ryr1^{+/+}$ and $Ryr1^{D/D}$ muscle fibers. Next we sought to evaluate Ca^{2+} handling properties in single intact $Ryr1^{+/+}$ ($n = 20$) and $Ryr1^{D/D}$ ($n = 22$) muscle fibers stimulated by an action potential. FDB fibers from 1.5-mo-old mice were loaded with the ratiometric Ca^{2+} indicator Indo-1 AM and stimulated with field electrodes. While the resting intracellular [Ca^{2+}] ([Ca^{2+}]$_i$) before stimulation was not significantly different between groups ($Ryr1^{+/+}$ = 0.662 ± 0.089 ratio, 79.7 ± 8.3 nM, $Ryr1^{D/D}$ = 0.6223 ± 0.144 ratio, 74.2 ± 11.5 nM, Fig. 7, *A* and *B*, *left*), there was a significant reduction in the cytosolic Ca^{2+} transient in mutant fibers following a single action potential ($Ryr1^{+/+}$ = 1.09 ± 0.06, $Ryr1^{D/D}$ = 0.86 ± 0.07, $P < 0.05$, Fig. 7*B*, *right*). These data are consistent with decreased activation of $Ryr1^{D/D}$ due to loss of binding of CaM, S100A1, or both CaM and S100A1.

Because CaCaM inhibits RyR1 when [Ca^{2+}]$_i$ becomes elevated, we next utilized a double-pulse protocol to evaluate transient responses at different times following a rise in [Ca^{2+}]$_i$. Following an initial conditioning stimulus, a second stimulus was given after 40, 80, or 160 ms of recovery (Fig. 7*C*). When normalized to the amplitude of the first transient elicited by the conditioning stimulus, the peak amplitude of the second Indo-1 transient was significantly increased following 40 ms recovery in $Ryr1^{D/D}$ fibers compared with their control counterparts ($P = 0.023$). This summation of the Ca^{2+} transient in mutant fibers became less pronounced as time allowed for recovery between stimuli increased (Fig. 7*C*).

Ultra-high-speed imaging of Fluo-4 Ca^{2+} transients and calculation of Ca^{2+} release flux following repetitive stimulation of $Ryr1^{+/+}$ and $Ryr1^{D/D}$ fibers. To allow for better temporal resolution of the Ca^{2+} transient summation seen in mutant fibers, we next monitored Fluo-4 transient responses following repetitive stimulation of $Ryr1^{+/+}$ and $Ryr1^{D/D}$ FDB

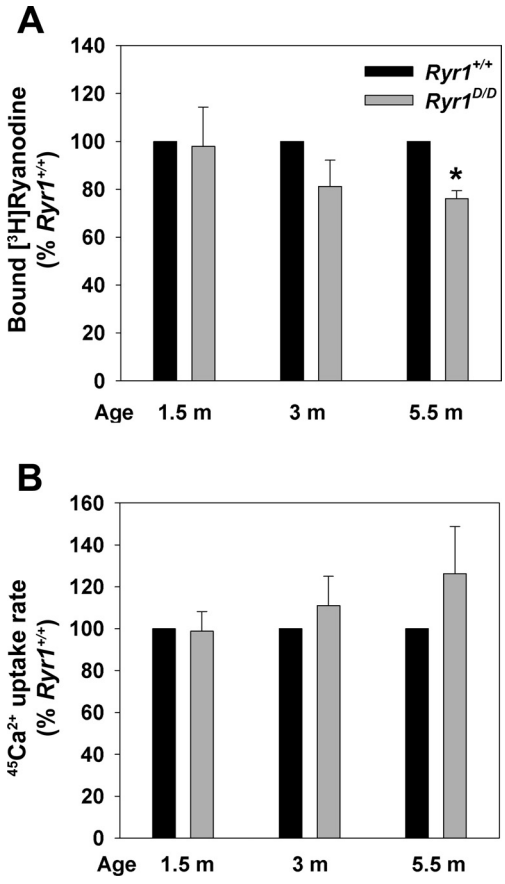

Fig. 6. Biochemical properties of membrane fractions isolated from $Ryr1^{+/+}$ and $Ryr1^{D/D}$ mice. *A*: maximal specific binding capacity (B_{max}) values of [^{3}H]ryanodine binding to crude skeletal muscle membrane fractions of 1.5- to 5.5-mo-old $Ryr1^{+/+}$ and $Ryr1^{D/D}$ mice were determined as described in EXPERIMENTAL PROCEDURES. Normalized data are means ± SE of 4–6 experiments. *$P < 0.05$ compared with $Ryr1^{+/+}$ mice. *B*: $^{45}Ca^{2+}$ uptake rates by crude membrane fractions of 1.5- to 5.5-mo-old $Ryr1^{+/+}$ and $Ryr1^{D/D}$ mice were determined as described in EXPERIMENTAL PROCEDURES. Normalized data are means ± SE of 4–5 experiments.

fibers using an ultra-high-speed (50 μs/line) line-scanning confocal microscope. Figure 8*A* demonstrates average responses from 18 control and 15 mutant fibers stimulated by a single action potential followed by a train of 10 action potentials at 100 Hz. Consistent with the Indo-1 data (Fig. 7), $Ryr1^{D/D}$ fibers demonstrated reduced amplitude of the fluorescent Ca^{2+} transient in response to single and tetanic action potential stimuli. However, when the traces were normalized to the amplitude of the first transient response, it was clear that there was greater relative summation of the Ca^{2+} transient during repetitive stimulation in the mutant fibers compared with control counterparts (Fig. 8*B*). Quantifying this summation as the ratio of the peak amplitude of the last transient to the first, the mutants demonstrated roughly twofold greater summation of $Ryr1^{+/+}$ fibers (Fig. 8*C*) ($Ryr1^{+/+} = 1.19 \pm 0.02$, $Ryr1^{D/D} = 1.41 \pm 0.03$; $P < 0.01$). Thus, the percent suppression of peak Fluo-4 fluorescence signal for a single pulse in the $Ryr1^{D/D}$ fibers was reversed by a factor of 1.41/1.19 by the time of the last transient in the train protocol of Fig. 8*B*.

To evaluate how the pronounced summation of fluorescent Ca^{2+} transients in mutant fibers translates to alterations in SR Ca^{2+} release, we utilized a Ca^{2+} removal model (20) to calculate the time course of SR Ca^{2+} release flux from action potential-evoked Fluo-4 Ca^{2+} transients. In essence, the properties of the binding sites (troponin C, parvalbumin) and reuptake system (SR Ca^{2+} pump) that remove free Ca^{2+} following release were empirically characterized from the decay of the fluorescent Ca^{2+} transient. The rate of SR Ca^{2+} release was then calculated as the time derivative of free, bound, and pumped Ca^{2+}. To characterize removal systems, we utilized a prolonged, high-frequency, repetitive stimulation protocol (a single action potential followed by 5 repeats of 200 ms, 100 Hz trains with 200 ms recovery between trains) to promote the saturation of cytosolic Ca^{2+} buffers (Fig. 9*A*). In accordance with previous protocols, $Ryr1^{D/D}$ fibers demonstrated approximately twofold greater relative summation of Ca^{2+} signals during the trains of repetitive stimuli, as seen in the normalized average recordings from 7 control and 10 mutant fibers in Fig. 9*A*. Figure 9*B* magnifies the last train in the series of five trains in Fig. 9*A* (box), and shows the average signals for fibers from $Ryr1^{+/+}$ and $Ryr1^{D/D}$ mice, normalized to the initial peak of the last train. Summation was then quantified as the ratio of the amplitude of the last peak in the train to the first peak. There was a significantly increased summation during the train of stimuli in $Ryr1^{D/D}$ fibers ($Ryr1^{+/+}$ summation = 1.55 ± 0.06, $n = 7$; $Ryr1^{D/D} = 1.97 \pm 0.1$, $n = 10$; $P < 0.01$). By fitting the decaying phase of the transient at the end of each train, and utilizing the same fixed and free parameters for uptake systems, release flux was calculated from individual fluorescence time courses of all mutant and control fibers. The average SR Ca^{2+} release flux time courses for $Ryr1^{+/+}$ and $Ryr1^{D/D}$ fibers are presented in Fig. 9*C*. Release flux was consistently suppressed throughout the stimulation paradigm in mutant fibers compared with controls, whereas the best-fit values of the free removal parameters were similar in the two groups of muscle fibers. $k_{on,P,Mg}$ and k_{uptake} were 0.0109 ± 0.0013 (means ± SE) μM/s and 2,818 ± 146 s^{-1} for WT ($N = 7$) and 0.0108 ± 0.0012 μM/s and 2,624 ± 159 s^{-1} for the mutant ($N = 10$), respectively.

Both groups demonstrate partial inactivation of release flux that essentially reaches a steady state during the trains of stimuli, as well as some cumulative suppression of release over the time course of the stimulation protocol. To measure the extent of the inactivation, we divided the peak release at the end of the first train (R_{end}) by the peak release elicited by the first action potential during the train (R_{first}). Fractional inactivation was calculated as $1 - (R_{end}/R_{first})$. Fractional inactivation was not significantly different between control and mutant fibers ($Ryr1^{+/+} = 0.819 \pm 0.009$, $Ryr1^{D/D} = 0.796 \pm 0.021$; $P > 0.05$). To quantify the kinetics of SR Ca^{2+} release inactivation, we fit the individual peaks of release flux elicited by the first train of stimuli in each record to a single-exponential function plus one constant (Fig. 9*D*). As demonstrated in Fig. 9*D*, the rate of inactivation was significantly slowed in $Ryr1^{D/D}$ fibers ($Ryr1^{+/+} = 7.93 \pm 0.4$ ms, $Ryr1^{D/D} = 12.2 \pm 1.6$ ms; $P < 0.05$). These results are consistent with CaM regulating the rate of inactivation of SR Ca^{2+} release flux via the CaM binding domain.

Voltage-clamp analysis of SR Ca^{2+} release flux in $Ryr1^{+/+}$ and $Ryr1^{D/D}$ fibers. To further characterize the effect of CaM regulation of release flux, we monitored fluorescence changes elicited by voltage-clamp depolarizations of Fluo-4-dialyzed $Ryr1^{+/+}$ and $Ryr1^{D/D}$ fibers. Fibers were dialyzed

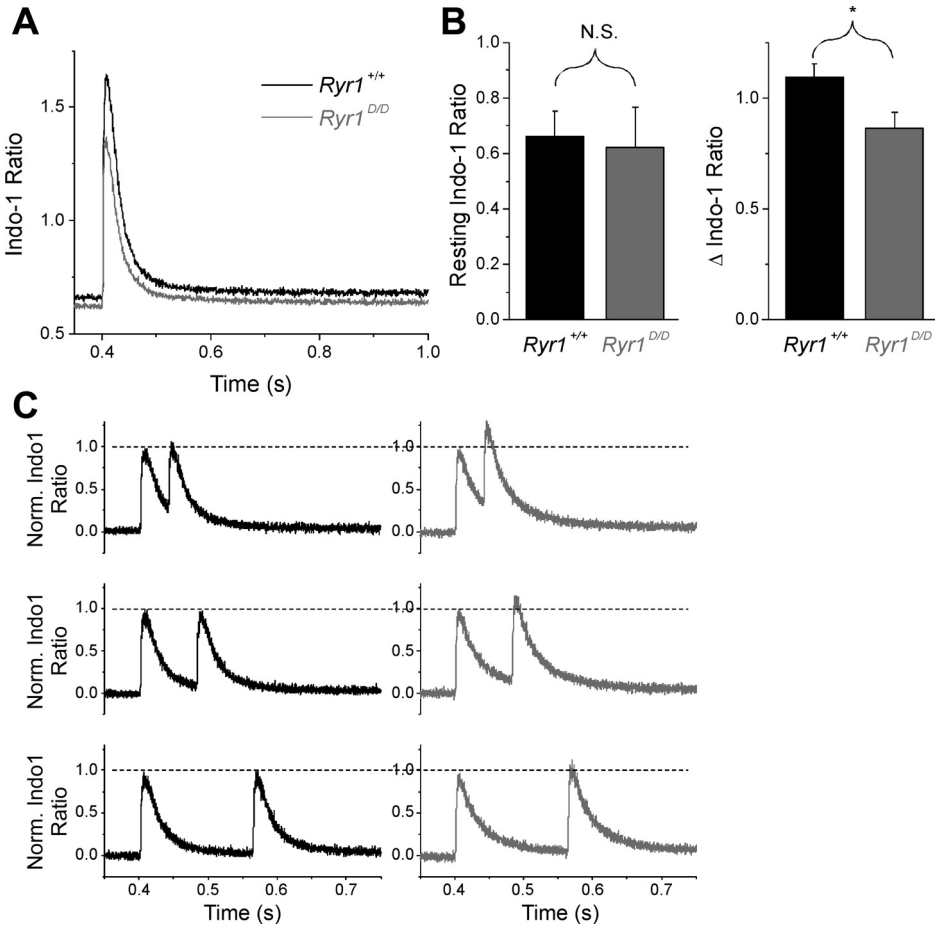

Fig. 7. *Ryr1*$^{D/D}$ muscle fibers exhibit normal Indo-1 resting ratio but decreased peak amplitude of the Indo-1 Ca^{2+} transient following a single action potential (AP). *A*: average Indo-1 ratio Ca^{2+} transients from *Ryr1*$^{+/+}$ (black trace; $n = 20$) and *Ryr1*$^{D/D}$ (gray trace; $n = 22$) fibers. Isolated fibers were stimulated with field electrodes at 400 ms, and emission ratio was examined. *B*: bar plot summarizing resting Indo-1 ratio averages (*left*) and peak ΔIndo-1 ratio (*right*) of control and mutant fibers. No significant (NS) differences in resting Ca^{2+} concentration were detected, but a significant difference in peak ΔIndo-1 ratio was found ($*P = 0.017$). *C*: averaged Indo-1 ratio responses from control (black traces; $n = 12$) and mutant (gray traces; $n = 12$) fibers elicited with a two-AP protocol with recovery periods of 40, 80, and 160 ms between stimuli. Traces were normalized to amplitude of the first stimulus to appreciate relative summation in mutant fibers.

with internal solution containing 20 mM EGTA and 50 μM Fluo-4 in the patch pipette for 20 min, and subjected to 80 ms depolarizing steps at 10-mV increments, starting from a holding potential of −80 mV. SR Ca^{2+} release flux was calculated from the resulting ΔF records in a procedure identical to that described (26). Consistent with previous reports, release flux at larger depolarizations consisted of a rapid rise to peak followed by a fast inactivation component, followed by a more slowly declining release for the duration of the pulse (Fig. 10*A*). As can be seen in the time course of release flux and in the release versus voltage (*R* vs. *V*) relationships (Fig. 10*A*), peak release flux was suppressed at all test voltages in the mutant fibers. The *R-V* relationship of control and mutant fibers was fit to a single Boltzmann function (Fig. 10*A*, *right*):

$$R(V) = R_{max}/\{1 + \exp[(V_{half} - V)/k]\} \quad (3)$$

with parameters R_{max} (maximum release flux), V_{half} (voltage of half-maximal activation), and k (slope factor). $R_{max} = 45.01 \pm 1.5$ μM/ms, $V_{half} = -11.9 \pm 1.7$ mV, $k = 9.4 \pm 1.63$ mV, for six control fibers, and $R_{max} = 26.5 \pm 4.3$ μM/ms, $V_{half} = -15.7 \pm 1.4$ mV, $k = 8.0 \pm 1.32$ mV, for eight mutant fibers. There was a 41% decrease in R_{max} in mutant *Ryr1*$^{D/D}$ fibers ($P < 0.05$).

To evaluate the kinetics of release flux, we compared the time course of release for control and mutant *Ryr1*$^{D/D}$ fibers at each voltage step, normalized to the peak amplitude of release. As can be seen in Fig. 10*B*, during the smaller depolarizations, such as to −20 mV (*left*), there were no noticeable differences in the relative time courses of release flux throughout the pulse. However, at larger depolarizations, such as to 0 mV (*middle*), a noticeable shoulder of sustained release was evident in the mutant *Ryr1*$^{D/D}$ muscle fibers during the fast inactivating phase. This shoulder became more pronounced at steeper depolarizations, where the fast inactivating component was more evident in control fibers and noticeably reduced in the mutant *Ryr1*$^{D/D}$ muscle fibers. Control and mutant fibers eventually reached a similar relative level of release flux by the end of the pulse. The results are consistent with CaCaM modulating the rapid inactivation of SR release flux during a depolarizing stimulus.

Contractile force measurements of Ryr1$^{+/+}$ *and Ryr1*$^{D/D}$ *mice in vivo.* We next assayed how alterations in Ca^{2+} release seen on a single fiber level translate to changes in whole muscle function of *Ryr1*$^{+/+}$ and *Ryr1*$^{D/D}$ mice in vivo. To measure function, we recorded maximal isometric contractile force produced by the TA muscles of anesthetized animals. Figure 11*A* shows representative twitch (single action potential stimulation) and maximal tetanic (100 Hz) force responses from *Ryr1*$^{+/+}$ and *Ryr1*$^{D/D}$ mice. One-hundred-hertz stimulation was used to elicit peak tetanic force, because greater stimulation frequencies resulted in a submaximal fused tetanus. As quantified in Fig. 11*C* and Table 1, mutant mice elicited a significant, 25% decrease in

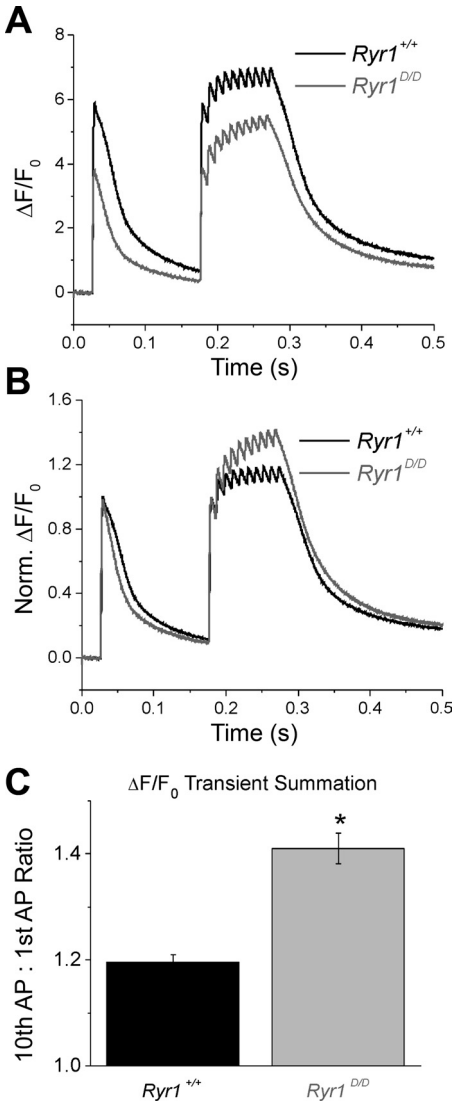

Fig. 8. *Ryr1*$^{D/D}$ muscle fibers exhibit pronounced summation of the Ca^{2+} transient during repetitive stimulation. *A*: Fluo-4 transient responses to single AP stimuli followed by a 100-Hz train of APs show reduced amplitude of Ca^{2+} twitch and tetanic transients in mutant fibers. *B*: traces from *A* normalized to initial transient amplitude to demonstrate greater summation of the Ca^{2+} transient during repetitive stimulation of mutant fibers when compared with controls. *C*: quantification of Ca^{2+} transient summation from *B*, calculated as the ratio of the amplitude of the last Ca^{2+} transient in the train compared with the first. Summation was increased approximately twofold in the mutant fibers. *$P < 0.01$.

twitch specific force (P_0) generated from a single action potential compared with WT controls. However, there was no difference in maximal tetanic P_0 generated between groups (Fig. 11*D*). This resulted in a significantly increased tetanus-to-twitch P_0 ratio in mutant mice, an indicator of greater relative force summation with repetitive activity (Fig. 11*E*). This is more clearly demonstrated in the normalized P_0 versus frequency of stimulation relationship depicted in Fig. 11*B*. At lower stimulation frequencies (10, 20, 40 Hz), *Ryr1*$^{D/D}$ mice demonstrated significantly less relative force; however, they showed greater relative summation at higher-frequency stimulation, which resulted in a similar maximal tetanic force response.

Next we sought to evaluate the maintenance of maximal force during prolonged repetitive fatiguing stimulation in *Ryr1*$^{+/+}$ and *Ryr1*$^{D/D}$ mice. The fatiguing paradigm and analysis were identical to that conducted previously in S100A1-knockout animals (24). Briefly, fatiguing stimulation consisted of 200 ms, 100 Hz trains to elicit maximal tetanic force, with a train spaced every 2 s for 300 s. Force was recorded continuously for each of the 150 tetani over the time of stimulation, and the percent reduction of force between the first and last train ($P_{0,final} - P_{0,initial}/P_{0,final}$) and the rate of force decline (fatigue tau) were calculated. No significant differences were seen in the rate of force decline or relative force decline between groups during fatiguing stimulation (Table 1). A summary of the biometrics and force data from contractile force experiments is detailed in Table 1. No significant differences were detected in body weight or muscle weight of the animals.

DISCUSSION

The present study describes a new mouse model for studying the in vivo regulation of RyR1 by CaM and S100A1. Previous studies with isolated membrane preparations and purified ryanodine receptors have suggested that CaM and S100A1 have a role in skeletal muscle EC coupling. However, the physiological significance of the regulation of RyR1 by these modulators remained unclear. Herein, we describe the creation and characterization of a genetically modified mouse with a single amino acid substitution in the CaM binding domain of RyR1 (RyR1-L3625D or RyR1^{D}). The position of the L3625D mutation is in the S100A1/CaM binding domain of RyR1 on the hydrophobic face of an amphipathic helix (Fig. 4). We previously expressed RyR1^{D} in HEK 293 cells and found that this single amino acid substitution was sufficient to inhibit CaM binding and regulation of the recombinant RyR1 mutant at submicromolar and micromolar Ca^{2+} (50). Similarly, the L3625D mutation abolished CaS100A1 binding to the S100A1/CaM binding domain of RyR1 (Fig. 4*E*). Results of the present study suggest that the L3625D mutation impairs CaM and S100A1 regulation of RyR1 in skeletal muscle, and thereby alters adult skeletal muscle EC coupling and force generation.

S100A1 has a significant role in skeletal muscle Ca^{2+} homeostasis by primarily regulating RyR1-mediated SR Ca^{2+} release (11). In agreement with an earlier study (43), S100A1 activated *Ryr1*$^{+/+}$ at nanomolar but not micromolar Ca^{2+}. Binding studies with fusion proteins revealed three S100A1

Table 1. *Descriptive statistics for contractile force measurements*

	n	Sex	Body Weight, g	TA Weight, mg	Twitch P_0, mN/mm^2	Tetanic P_0, mN/mm^2	Fatigue, %	Fatigue Tau (s)
Ryr1$^{+/+}$	5	3M, 2F	22.62 ± 1.16	35.8 ± 2.17	60.2 ± 6.0	176.0 ± 22.6	64.8 ± 4.8	103.8 ± 8.8
Ryr1$^{D/D}$	6	3F, 3M	20.81 ± 1.26	33.57 ± 2.10	*45.3 ± 3.3	188 ± 19.7	59.9 ± 5.2	86.3 ± 2.6

Values are means ± SE. M, male; F, female; TA, tibialis anterior; P_0, specific force. *$P < 0.05$.

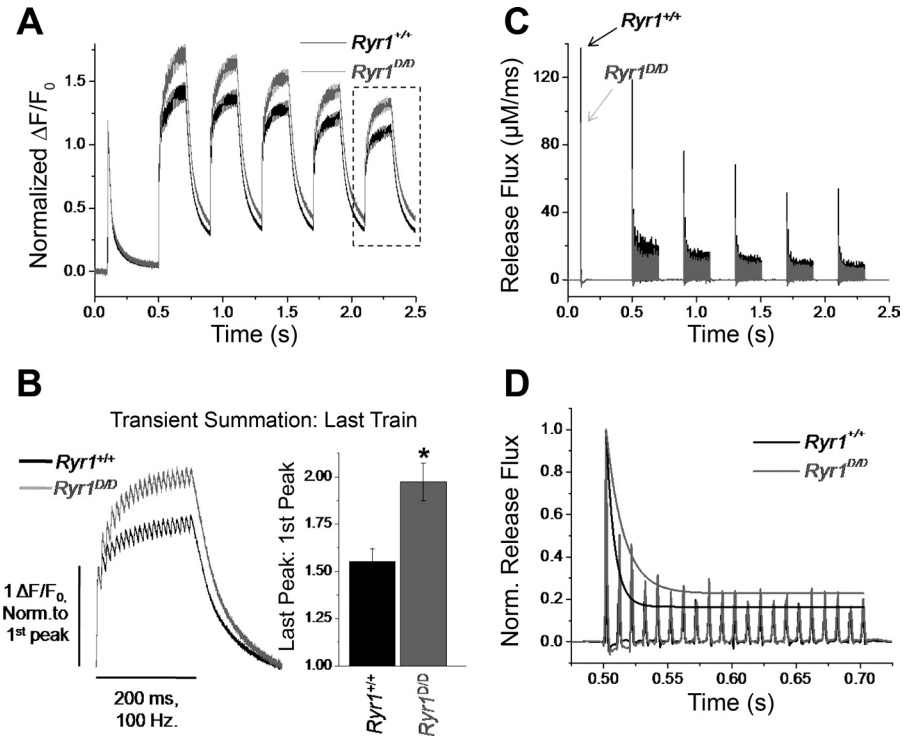

Fig. 9. *Ryr1*$^{D/D}$ muscle fibers demonstrate summation of AP-evoked Ca^{2+} transients and slower inactivation of sarcoplasmic reticulum (SR) Ca^{2+} release flux during tetanic stimulation. *A*: average Fluo-4 transient responses of 7 control and 10 mutant fibers to a single AP stimuli followed by 5 repeats of 200 ms trains of 100 Hz stimuli, with 200 ms recovery between trains. Traces are normalized to the amplitude of the first transient to demonstrate differences in transient summation during repetitive stimulation. *B*, *left*: boxed traces from *A*, time expanded and normalized to amplitude of the initial peak to examine transient summation of last train. *Right*: quantification of transient facilitation between *Ryr1*$^{+/+}$ and *Ryr1*$^{D/D}$ fibers (*$P < 0.01$, *Ryr1*$^{+/+}$ $n = 7$, *Ryr1*$^{D/D}$ $n = 10$). *C*: average SR Ca^{2+} release flux of control and mutant fibers, quantified using a Ca^{2+} removal model to calculate release from fluorescence responses of fibers subjected to stimulation paradigm seen in *A*. Release flux is suppressed in mutant fibers compared with controls. *D*: representative SR Ca^{2+} release flux time course of first tetanic train in *C* from a control and mutant fiber, normalized to amplitude of initial flux. Peaks of release flux are fit to a single exponential function to quantify inactivation of release during the train. Tau of inactivation is significantly increased in *Ryr1*$^{D/D}$ fibers, suggesting a slower rate of inactivation. Fractional inactivation was not significantly different between the groups.

binding sites, one of which overlapped with the Ca^{2+}-dependent CaM binding site of RyR1. The present study shows that the functional effects of S100A1 in WT are mediated through a single binding site shared by CaM. *Ryr1*$^{+/+}$ channels were activated by 0.3 μM S100A1, which is within the concentration range of S100A1 protein concentration in fast-twitch skeletal muscle (15, 52). However, it will be important to establish in future studies the local concentrations of free S100A1 and CaM available to bind RyR1 at the triad junction, because these likely determine relative binding and competition at this site in vivo.

S100A1 binds to the NH_2-terminal region of the CaM binding domain involved in the binding of the Ca^{2+}-bound form of CaM to RyR1 (17, 30). The apparent discrepancy of binding to this region at submicromolar Ca^{2+} concentrations can be explained by the fact that binding to RyR1 increases the Ca^{2+} binding affinity of S100A1, as demonstrated for S100 family members in the presence of various target proteins (16, 46). We suggest that at resting Ca^{2+} concentrations, in agreement with binding (47, 50) and single-channel (Figs. 2 and 5) studies, RyR1 may be activated by S100A1 and CaM, whereas at elevated Ca^{2+} concentrations, following a train of action potentials, CaM but not S100A1 inhibits RyR1.

The RyR1-L3625D mutant mice provided membrane fractions that contained the two key SR Ca^{2+} transport systems, RyR1 and the ATP-dependent Ca^{2+} pump. An impaired activation of RyR1 by S100A1 and CaM suggests that depressed Ca^{2+} transients observed in mutant fibers in response to a voltage stimulus are in part due to expression of dysfunctional RyR1. Our data also support the idea that diminished CaM inhibition of the mutant RyR1 ion channel increased the summation of Ca^{2+} transients in *Ryr1*$^{D/D}$ fibers. Because the $^{45}Ca^{2+}$ uptake rate was similar in WT and mutant membrane preparations, it seems unlikely that a decreased Ca^{2+} pump activity causes a reduced rate of cytosolic Ca^{2+} removal in *Ryr1*$^{D/D}$ mice, consistent with no change in removal properties in the Ca^{2+} transient measurements.

It is notable that the depressed Ca^{2+} transients observed in mutant fibers had no major effect on the behavior of the mutant mice. The mutant mice were viable and had an apparently normal lifespan, as is also seen in *S100A1*$^{-/-}$ mice. The results support the idea that while not essential for skeletal muscle EC coupling, CaM and S100A1 tune SR Ca^{2+} release to regulate muscle function. The lack of a major effect on sustained performance during repetitive or fatiguing stimulation may appear surprising, given the significantly altered SR Ca^{2+} handling in mutant mice. This may be due to the fact that *Ryr1*$^{D/D}$ mice have impaired regulation by two activators (CaM and S100A1) and an inhibitor (CaM) of SR Ca^{2+} release (see below). The result of removing the activating effect was seen directly in the diminished Ca^{2+} transient in response to a single action potential in fibers from the *Ryr1*$^{D/D}$ mice. On the other hand, repetitive stimulation of fibers and muscles from *Ryr1*$^{D/D}$ mice exhibited increased relative summation of Ca^{2+} signals during the train, so that the suppression of myoplasmic Ca^{2+} in fibers from *Ryr1*$^{D/D}$ mice was less at the end than at the start of the train. This was consistent with the elimination of an inactivating effect of CaM in fibers from *Ryr1*$^{D/D}$ mice. The combination of these two opposing effects may partially explain the lack of effect of this mutation during repetitive muscular activity in *Ryr1*$^{D/D}$ mice. In contrast, muscles from *S100A1*$^{-/-}$ animals showed decreased contractile force for a single action potential as well as decreased force during repetitive stimulation (24), suggesting that S100A1 activation is required to maintain in vivo muscle performance.

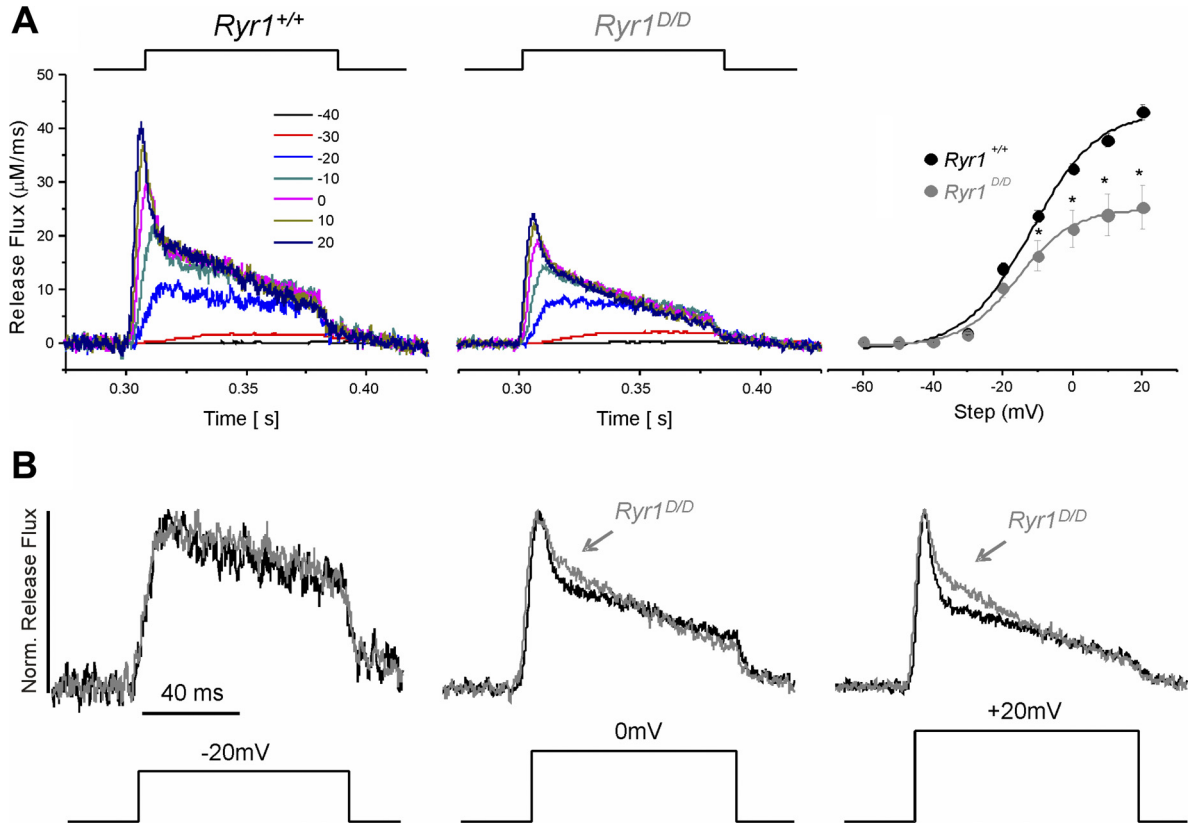

Fig. 10. *Ryr1*$^{D/D}$ muscle fibers exhibit reduced Ca^{2+} release flux with slowed inactivation of Ca^{2+} release in response to voltage-clamp depolarizations. *A*: average Ca^{2+} release flux from control (*left*; $n = 6$) and *Ryr1*$^{D/D}$ (*middle*; $n = 8$) fibers calculated from Fluo-4 fluorescent transients elicited by steplike 80-ms depolarizations from a holding potential of −80 mV. At *right* is the release vs. voltage (*R-V*) relationships of control and *Ryr1*$^{D/D}$ fibers. SR Ca^{2+} release flux was significantly suppressed in mutant muscle fibers. $*P < 0.05$. *B*: Ca^{2+} release flux from *A* elicited by depolarizing pulses to −20, 0, and +20 mV from a holding potential of −80 mV, normalized to peak flux to investigate the relative time course of Ca^{2+} release. While the time course of release was similar between mutant and control fibers at lesser depolarizations (−20 mV, *left*), upon larger depolarizations (0 mV, +20 mV), mutant fibers demonstrate less rapid inactivation of release compared with controls, as seen by the pronounced shoulder during the fast inactivation of release flux in *Ryr1*$^{D/D}$ fibers.

Comparison of the present results in RyR1-L3625D mice with those from *S100A1*$^{-/-}$ animals provides some insight into the roles of S100A1 and CaM in skeletal muscle EC coupling. The 41% average decrease in peak SR Ca^{2+} release flux during voltage-clamp depolarization of FDB fibers from *Ryr1*$^{D/D}$ mice (Fig. 10) was remarkably similar to the 42% average decrease in release flux seen in FDB fibers from *S100A1*$^{-/-}$ mice under identical conditions (25, 26). Furthermore, both Indo-1 and Fluo-4 recordings of Ca^{2+} transients elicited by single action potentials showed similarly reduced amplitudes in *Ryr1*$^{D/D}$ (Figs. 7 and 8) and *S100A1*$^{-/-}$ muscle fibers (27). There is also a similar decrease in contractile twitch force between *Ryr1*$^{D/D}$ (Fig. 11) and *S100A1*$^{-/-}$ mice (24). Considering that S100A1 primarily regulates RyR1 in skeletal muscle (11), our findings suggest two important concepts. First, elimination of the S100A1 activating effects on RyR1 appears to fully account for the suppressed release flux and twitch force generation in *Ryr1*$^{D/D}$ mutant mice. Second, suppressed Ca^{2+} release in *S100A1*$^{-/-}$ fibers is likely attributable to impaired S100A1 regulation of RyR1 specifically at the CaM binding site. Conversely, the decreased summation of Ca^{2+} transients and force seen during repetitive stimulation in *S100A1*$^{-/-}$ muscle may be attributed to the lack of competition of S100A1 with the inhibitory action of CaCaM at this same binding site on RyR1.

In contrast to a predominant role S100A1 may have in promoting channel activation from rest, a clear role for CaCaM regulation of release flux becomes evident as cytosolic [Ca^{2+}] increases in *Ryr1*$^{D/D}$ mice during maintained fiber stimulation. In response to sustained depolarization, there was a shoulder of prolonged Ca^{2+} release flux in *Ryr1*$^{D/D}$ fibers. Importantly, this "shoulder" was markedly absent in S100A1-deficient fibers exposed to the same depolarizing step (25, 26), suggesting that impaired CaCaM inactivation of RyR1 likely accounts for the prolonged release in *Ryr1*$^{D/D}$ fibers. Consistent with an inhibitory role of CaCaM, *Ryr1*$^{D/D}$ fibers show a pronounced Ca^{2+} transient summation and slowed inactivation of release flux in response to trains of action potentials (Figs. 8 and 9). *S100A1*$^{-/-}$ fibers demonstrate the opposite effects of reduced transient summation and greater inactivation of release flux during prolonged trains of action potentials (24). This suggests that CaCaM may have an inhibitory role in *S100A1*$^{-/-}$ fibers, due to the lack of regulation of RyR1 by endogenous S100A1.

The RyR1 CaM binding domain has a cysteine (Cys3635) that is *S*-nitrosylated by low, physiological concentrations (0.75 μM) of nitric oxide (NO) (38). Activation of RyR1 by NO was observed at Po_2 of ~10 mmHg (simulating muscle oxygen tension) in the presence but not absence of CaM (38). This suggests that an impaired CaM binding renders *Ryr1*$^{D/D}$ insensitive to NO activation.

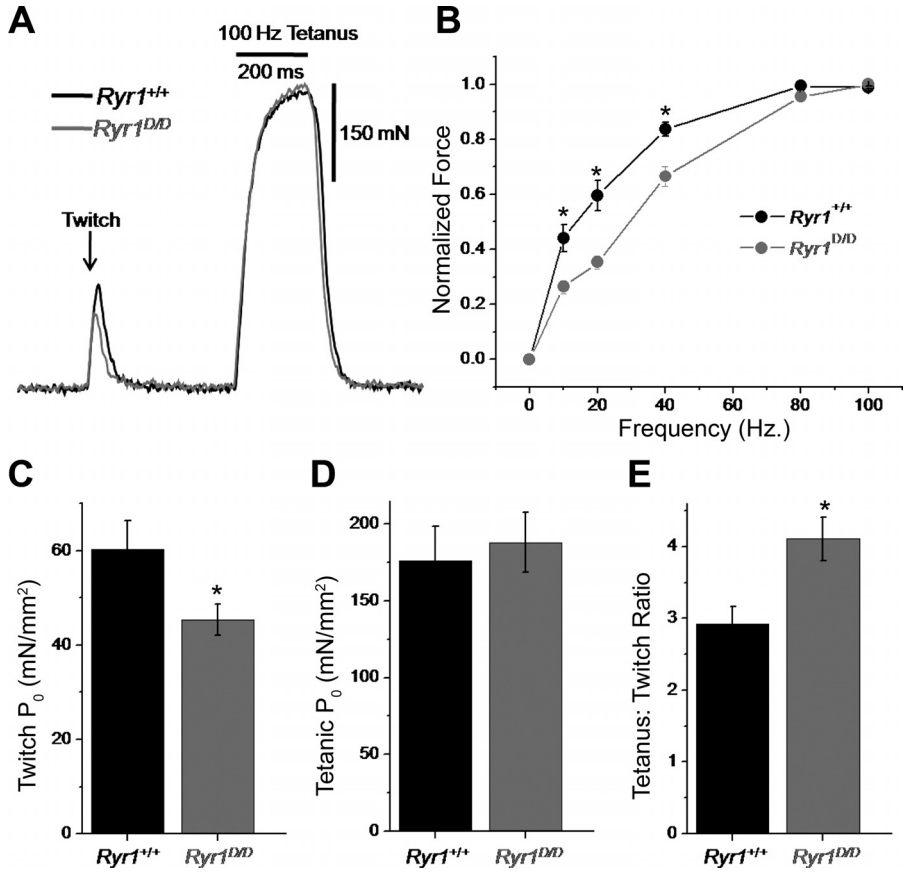

Fig. 11. $Ryr1^{D/D}$ mice exhibit decreased twitch force generation and increased force summation in vivo. *A*: representative twitch (single AP) and tetanic (100 Hz, 200 ms) force responses from the tibialis anterior muscles of anesthetized $Ryr1^{+/+}$ and $Ryr1^{D/D}$ mice. *B*: force vs. frequency of stimulation relationships for $Ryr1^{+/+}$ ($n = 5$) and $Ryr1^{D/D}$ ($n = 6$) mice. *C*: specific twitch force of $Ryr1^{+/+}$ and $Ryr1^{D/D}$ mice. *D*: specific tetanic force of $Ryr1^{+/+}$ and $Ryr1^{D/D}$ mice. *E*: tetanus-to-twitch ratio, an indicator of summation, of $Ryr1^{+/+}$ and $Ryr1^{D/D}$ mice. $^*P < 0.05$

The effects of eliminating the interaction of CaM with the ryanodine receptors were previously examined in cardiac muscle. We generated a mutant mouse deficient in the regulation by CaM of the cardiac ryanodine receptor isoform ($Ryr2^{ADA/ADA}$ mouse) (49). Mice that expressed only the mutant form of RyR2 showed signs of cardiac hypertrophy as early as 1 day after birth and died ~2 wk later. Sustained Ca^{2+} transients were observed in cultured homozygous cardiomyocytes isolated from 1-day-old mice. The results indicate that impaired CaM and likely S100A1 regulation of the ryanodine receptors has markedly different effects in cardiac and skeletal muscle. One possible explanation is that the two isoforms are differently regulated by CaM and S100A1. In contrast to $Ryr2^{ADA/ADA}$ mice, $S100A1^{-/-}$ mice have a normal lifespan and cardiac function under baseline conditions (6), which suggests a predominant role of CaM regulation of RyR2 compared with S100A1 in cardiac muscle. In cardiac failure, S100A1 protein levels are decreased (28, 44). Gene expression restored cardiac function in a rat model of heart failure (23), and transgenic overexpression in the heart increased myocardial performance (21). Differences in the regulation between RyR1 and RyR2 may be also due to the expression and greater role in Ca^{2+} signaling of RyR2 during early development. Mutant mice lacking RyR2 die at approximately *embryonic day 10* (41), whereas mutant mice lacking a functional RyR1 are viable until birth (40).

In cardiac muscle, S100A1 interacts with multiple targets including RyR2 and Ca^{2+}-ATPase (SERCA2a) and its regulatory protein, phospholamban (11, 46). S100A1 has been found to both inhibit and activate RyR2 (10, 45) and to bind to a peptide containing part of the conserved CaM binding site of RyR1 and RyR2 (47). However, the interaction sites for S100A1 in the intact RyR2, and their potential loss in the $Ryr2^{ADA/ADA}$ mutant mouse, remain to be determined.

In summary, at nanomolar Ca^{2+} concentrations CaM and S100A1 activate RyR1 in single-channel measurements. Regulation involves a shared binding site in RyR1. On the other hand, only CaM inhibits RyR1 at micromolar Ca^{2+} concentrations. CaM and S100A1 regulation tunes SR Ca^{2+} release to differentially regulate EC coupling during high- and low-frequency stimulation. However, how CaM and S100A1 compete for the site under physiological and pathological conditions in skeletal muscle and other tissues to regulate Ca^{2+} release from intracellular Ca^{2+} stores requires further investigation.

ACKNOWLEDGMENTS

We thank Dr. Oliver Smithies for advice and reagents in creating the $Ryr1^{D/D}$ mouse and Dr. Zoita Andronache for helpful discussions.

Present Address for N. Yamaguchi, Department of Regenerative Medicine and Cell Biology, Medical University of South Carolina, Charleston, SC 29425.

GRANTS

Support of National Institutes of Health Grants HL081825 (to J. P. Eu), AR053235 and AR059179 (to R. M. Lovering), GM58888 (to D. Weber), AR055099 (to M. F. Schneider), and AR018687 (to G. Meissner) and Deutsche Forschungsgemeinschaft Grant ME 713/18 (to W. Melzer) is gratefully acknowledged.

DISCLOSURES

No conflicts of interest, financial or otherwise, are declared by the authors.

REFERENCES

1. **Balshaw DM, Xu L, Yamaguchi N, Pasek DA, Meissner G.** Calmodulin binding and inhibition of cardiac muscle calcium release channel (ryanodine receptor). *J Biol Chem* 276: 20144–20153, 2001.
2. **Balshaw DM, Yamaguchi N, Meissner G.** Modulation of intracellular calcium release channels by calmodulin. *J Membr Biol* 185: 1–8, 2002.
3. **Baylor SM, Hollingworth S.** Sarcoplasmic reticulum calcium release compared in slow-twitch and fast-twitch fibres of mouse muscle. *J Physiol* 551: 125–138, 2003.
4. **Bronson SK, Plaehn EG, Kluckman KD, Hagaman JR, Maeda N, Smithies O.** Single-copy transgenic mice with chosen-site integration. *Proc Natl Acad Sci USA* 93: 9067–9072, 1996.
5. **Bunting M, Bernstein KE, Greer JM, Capecchi MR, Thomas KR.** Targeting genes for self-excision in the germ line. *Genes Dev* 15: 1524–1528, 1999.
6. **Du XJ, Cole TJ, Tenis N, Gao XM, Kontgen F, Kemp BE, Heierhorst J.** Impaired cardiac contractility response to hemodynamic stress in S100A1-deficient mice. *Mol Cell Biol* 22: 2821–2829, 2002.
7. **Fill M, Copello JA.** Ryanodine receptor calcium release channels. *Physiol Rev* 82: 893–922, 2002.
8. **Franzini-Armstrong C, Protasi F.** Ryanodine receptors of striated muscles: a complex channel capable of multiple interactions. *Physiol Rev* 77: 699–729, 1997.
9. **Harkins AB, Kurebayashi N, Baylor SM.** Resting myoplasmic free calcium in frog skeletal muscle fibers estimated with fluo-3. *Biophys J* 65: 865–881, 1993.
10. **Kettlewell S, Most P, Currie S, Koch WJ, Smith GL.** S100A1 increases the gain of excitation-contraction coupling in isolated rabbit ventricular cardiomyocytes. *J Mol Cell Cardiol* 39: 900–910, 2005.
11. **Kraus C, Rohde D, Weidenhammer C, Qiu G, Pleger ST, Voelkers M, Boerries M, Remppis A, Katus HA, Most P.** S100A1 in cardiovascular health and disease: closing the gap between basic science and clinical therapy. *J Mol Cell Cardiol* 47: 445–455, 2009.
12. **Ledbetter MW, Preiner JK, Louis CF, Mickelson JR.** Tissue distribution of ryanodine receptor isoforms and alleles determined by reverse transcription polymerase chain reaction. *J Biol Chem* 269: 31544–31551, 1994.
13. **Liu Y, Carroll SL, Klein MG, Schneider MF.** Calcium transients and calcium homeostasis in adult mouse fast-twitch skeletal muscle fibers in culture. *Am J Physiol Cell Physiol* 272: C1919–C1927, 1997.
14. **Lovering RM, De Deyne PG.** Contractile function, sarcolemma integrity, and the loss of dystrophin after skeletal muscle eccentric contraction-induced injury. *Am J Physiol Cell Physiol* 286: C230–C238, 2004.
15. **Maco B, Brezova A, Schafer BW, Uhrik B, Heizmann CW.** Localization of the Ca^{2+}-binding S100A1 protein in slow and fast skeletal muscles of the rat. *Gen Physiol Biophys* 16: 373–377, 1997.
16. **Markowitz J, Rustandi RR, Varney KM, Wilder PT, Udan R, Wu SL, Horrocks WD, Weber DJ.** Calcium-binding properties of wild-type and EF-hand mutants of S100B in the presence and absence of a peptide derived from the C-terminal negative regulatory domain of p53. *Biochemistry* 44: 7305–7314, 2005.
17. **Maximciuc AA, Putkey JA, Shamoo Y, MacKenzie KR.** Complex of calmodulin with the ryanodine receptor target reveals a novel, flexible binding mode. *Structure* 14: 1547–1556, 2006.
18. **Meissner G.** Regulation of mammalian ryanodine receptors. *Front Biosci* 7: d2072–d2080, 2002.
19. **Melzer W, Rios E, Schneider MF.** The removal of myoplasmic free calcium following calcium release in frog skeletal muscle. *J Physiol* 372: 261–292, 1986.
20. **Melzer W, Rios E, Schneider MF.** A general procedure for determining the rate of calcium release from the sarcoplasmic reticulum in skeletal muscle fibers. *Biophys J* 51: 849–863, 1987.
21. **Most P, Remppis A, Pleger ST, Loffler E, Ehlermann P, Bernotat J, Kleuss C, Heierhorst J, Ruiz P, Witt H, Karczewski P, Mao L, Rockman HA, Duncan SJ, Katus HA, Koch WJ.** Transgenic overexpression of the Ca^{2+} binding protein S100A1 in the heart leads to increased in vivo myocardial contractile performance. *J Biol Chem* 278: 33809–33817, 2003.
22. **O'Connell KM, Yamaguchi N, Meissner G, Dirksen RT.** Calmodulin binding to the 3614–3643 region of RyR1 is not essential for excitation-contraction coupling in skeletal myotubes. *J Gen Physiol* 120: 337–347, 2002.
23. **Pleger ST, Most P, Boucher M, Soltys S, Chuprun JK, Pleger W, Gao E, Dasgupta A, Rengo G, Remppis A, Katus HA, Eckhart AD, Rabinowitz JE, Koch WJ.** Stable myocardial-specific AAV6–S100A1 gene therapy results in chronic functional heart failure rescue. *Circulation* 115: 2506–2515, 2007.
24. **Prosser BL, Hernandez-Ochoa EO, Lovering RM, Andronache Z, Zimmer DB, Melzer W, Schneider MF.** S100A1 promotes action potential-initiated calcium release flux and force production in skeletal muscle. *Am J Physiol Cell Physiol* 299: C891–C902, 2010.
25. **Prosser BL, Hernandez-Ochoa EO, Zimmer DB, Schneider MF.** The Qgamma component of intra-membrane charge movement is present in mammalian muscle fibres, but suppressed in the absence of S100A1. *J Physiol* 587: 4523–4541, 2009.
26. **Prosser BL, Hernandez-Ochoa EO, Zimmer DB, Schneider MF.** Simultaneous recording of intramembrane charge movement components and calcium release in wild-type and S100A1−/− muscle fibres. *J Physiol* 587: 4543–4559, 2009.
27. **Prosser BL, Wright NT, Hernandez-Ochoa EO, Varney KM, Liu Y, Olojo R, Zimmer DB, Weber DJ, Schneider MF.** S100A1 binds to the calmodulin-binding site of ryanodine receptor and modulates skeletal muscle excitation-contraction coupling. *J Biol Chem* 283: 5046–5057, 2008.
28. **Remppis A, Greten T, Schäfer BW, Hunziker P, Erne P, Katus HA, Heizmann CW.** Altered expression of the Ca^{2+}-binding protein S100A1 in human cardiomyopathy. *Biochim Biophys Acta* 1313: 253–257, 1996.
29. **Rodney GG.** Calmodulin in adult mammalian skeletal muscle: Localization and effect on sarcoplasmic reticulum Ca^{2+} release. *Am J Physiol Cell Physiol* 294: C1288–C1297, 2008.
30. **Rodney GG, Moore CP, Williams BY, Zhang JZ, Krol J, Pedersen SE, Hamilton SL.** Calcium binding to calmodulin leads to an N-terminal shift in its binding site on the ryanodine receptor. *J Biol Chem* 276: 2069–2074, 2001.
31. **Radzyukevich TL, Cougnon MH, Moseley AE, Heiny JA.** Developmental induction of DHPR alpha 1s and RYR1 gene expression does not require neural or mechanical signals. *J Muscle Res Cell Motil* 2004: 87–94, 2004.
32. **Samso M, Wagenknecht T.** Apocalmodulin and Ca^{2+}-calmodulin bind to neighboring locations on the ryanodine receptor. *J Biol Chem* 277: 1349–1353, 2002.
33. **Schneider MF, Chandler WK.** Voltage dependent charge movement in skeletal muscle: a possible step in excitation-contraction coupling. *Nature* 242: 244–246, 1973.
34. **Schoenmakers TJ, Visser GJ, Flik G, Theuvenet AP.** CHELATOR: an improved method for computing metal ion concentrations in physiological solutions. *Biotechniques* 12: 870–879, 1992.
35. **Schuhmeier RP, Dietze B, Ursu D, Lehmann-Horn F, Melzer W.** Voltage-activated calcium signals in myotubes loaded with high concentrations of EGTA. *Biophys J* 84: 1065–1078, 2003.
36. **Schuhmeier RP, Melzer W.** Voltage-dependent Ca^{2+} fluxes in skeletal myotubes determined using a removal model analysis. *J Gen Physiol* 123: 33–51, 2004.
37. **Shirokova N, Garcia J, Pizarro G, Rios E.** Ca^{2+} release from the sarcoplasmic reticulum compared in amphibian and mammalian skeletal muscle. *J Gen Physiol* 107: 1–18, 1996.
38. **Sun J, Xin C, Eu JP, Stamler JS, Meissner G.** Cysteine-3635 is responsible for skeletal muscle ryanodine receptor modulation by NO. *Proc Natl Acad Sci USA* 98: 11158–11162, 2001.
39. **Sutko JL, Airey JA, Welch W, Ruest L.** The pharmacology of ryanodine and related compounds. *Pharmacol Rev* 49: 53–98, 1997.
40. **Takeshima H, Iino M, Takekura H, Nishi M, Kuno J, Minowa O, Takano H, Noda T.** Excitation-contraction uncoupling and muscular degeneration in mice lacking functional skeletal muscle ryanodine-receptor gene. *Nature* 369: 556–559, 1994.
41. **Takeshima H, Komazaki S, Hirose K, Nishi M, Noda T, Iino M.** Embryonic lethality and abnormal cardiac myocytes in mice lacking ryanodine receptor type 2. *EMBO J* 1998: 3309–3316, 1998.
42. **Timmer J, Müller T, Melzer W.** Numerical methods to determine calcium release flux from calcium transients in muscle cells. *Biophys J* 74: 1694–1707, 1998.
43. **Treves S, Scutari E, Robert M, Groh S, Ottolia M, Prestipino G, Ronjat M, Zorzato F.** Interaction of S100A1 with the Ca^{2+} release channel (ryanodine receptor) of skeletal muscle. *Biochemistry* 36: 11496–11503, 1997.

44. **Tsoporis JN, Marks A, Zimmer DB, McMahon C, Parker TG.** The myocardial protein S100A1 plays a role in the maintenance of normal gene expression in the adult heart. *Mol Cell Biochem* 242: 27–33, 2003.
45. **Volkers M, Loughrey CM, Macquaide N, Remppis A, DeGeorge BR Jr, Wegner FV, Friedrich O, Fink RH, Koch WJ, Smith GL, Most P.** S100A1 decreases calcium spark frequency and alters their spatial characteristics in permeabilized adult ventricular cardiomyocytes. *Cell Calcium* 41: 135–143, 2007.
46. **Wright NT, Cannon BR, Zimmer DB, Weber DJ.** S100A1: structure, function, and therapeutic potential. *Curr Chem Biol* 3: 138–145, 2009.
47. **Wright NT, Prosser BL, Varney KM, Zimmer DB, Schneider MF, Weber DJ.** S100A1 and calmodulin compete for the same binding site on ryanodine receptor. *J Biol Chem* 283: 26676–26683, 2008.
48. **Xu L, Tripathy A, Pasek DA, Meissner G.** Ruthenium red modifies the cardiac and skeletal muscle Ca^{2+} release channels (ryanodine receptors) by multiple mechanisms. *J Biol Chem* 274: 32680–32691, 1999.
49. **Yamaguchi N, Takahashi N, Xu L, Smithies O, Meissner G.** Early cardiac hypertrophy in mice with impaired calmodulin regulation of cardiac muscle Ca^{2+} release channel. *J Clin Invest* 117: 1344–1353, 2007.
50. **Yamaguchi N, Xin C, Meissner G.** Identification of apocalmodulin and Ca^{2+}-calmodulin regulatory domain in skeletal muscle Ca^{2+} release channel, ryanodine receptor. *J Biol Chem* 276: 22579–22585, 2001.
51. **Yamaguchi N, Xu L, Pasek DA, Evans KE, Chen SR, Meissner G.** Calmodulin regulation and identification of calmodulin binding region of type-3 ryanodine receptor calcium release channel. *Biochemistry* 44: 15074–15081, 2005.
52. **Zimmer DB.** Examination of the calcium-modulated protein S100 alpha and its target proteins in adult and developing skeletal muscle. *Cell Motil Cytoskeleton* 20: 325–237, 1991.